Available online at www.sciencedirect.com
ScienceDirect
Coordination Chemistry Reviews 251 (2007) 429–453
COORDINATION CHEMISTRY REVIEWS
www.elsevier.com/locate/ccr

Review

Application of MCD spectroscopy to porphyrinoids

John Mack [a,b], Martin J. Stillman [b,*], Nagao Kobayashi [a,*]

[a] *Department of Chemistry, Graduate School of Science, Tohoku University, Sendai 980-8578, Japan*
[b] *Department of Chemistry, University of Western Ontario, London, Ontario, Canada N6A 5B7*

Received 6 March 2006; accepted 22 May 2006
Available online 2 June 2006

Contents

Abstract

Magnetic circular dichroism (MCD) spectroscopy has proven invaluable in the assignment of the optical spectra of the porphyrinoids over the last 40 years. Recently, with new power of the DFT theoretical treatments available routinely, the assignment of porphyrinoid spectra has become an important factor in the correct interpretation of the electronic structure predicted by the calculations. In this review, we have described in detail the formalism required to use the MCD technique to probe the electronic structure of porphyrinoid complexes. We begin with a detailed description of the optical background to the technique; continue by describing the current theoretical interpretation of the spectral morphology, and end by describing the analysis of the MCD spectral data for a number of porphyrins and phthalocyanines.

Keywords: Porphyrin; Phthalocyanine; MCD spectroscopy; MO calculations; DFT; INDO

Abbreviations: ΔA_{l-r}, differential absorbance of lcp and rcp light; Δ_{OCT}, ligand field splitting; ΔHOMO, splitting of the π-system MOs derived from the $1e_{4u}$ HOMO of the parent $C_{16}H_{16}^{2-}$ hydrocarbon perimeter in eV; ΔLUMO, splitting of the π-system MOs derived from the $1e_{5g}^{*}$ HOMO of the parent $C_{16}H_{16}^{2-}$ hydrocarbon perimeter in eV; AO, atomic orbital; CD, circular dichroism; *D*, axial ZFS parameter; *E*, rhombic ZFS parameter; HOMO, highest occupied molecular orbital; LCAO, linear combination of atomic orbitals; LUMO, lowest unoccupied molecular orbital; lcp, left circularly polarized; MCD, magnetic circular dichroism; MO, molecular orbital; MORD, magnetic optical rotatory dispersion; NMR, nuclear magnetic resonance; OEP, octaethylporphyrin; OAM, orbital angular momentum; ORD, optical rotatory dispersion; Pc, phthalocyanine; rcp, right circularly polarized; TPP, tetraphenylporphyrin; VB, valence bond; VTVF, variable temperature variable field; ZFS, zero field splitting

* Corresponding authors. Tel.: +1 519 661 3821; fax: +1 519 661 3022.
E-mail address: Stillman@uwo.ca (M.J. Stillman).

0010-8545/$ – see front matter © 2006 Elsevier B.V. All rights reserved.
doi:10.1016/j.ccr.2006.05.011

1. Introduction

The synthesis, electrochemistry and optical spectroscopy of metal porphyrinoid complexes and their cation and anion radical species, has been a major research focus of both the Stillman and Kobayashi research groups over the past three decades [1]. Naturally occurring porphyrinoid ligands, Fig. 1, play a key role in biological redox processes such as photosynthesis and respiration. The electrochemistry, photochemistry and ligand-binding chemistry of chlorophylls, hemes, and the corrin within Vitamin B_{12}, has, therefore, inspired a variety of high technology applications for porphyrinoids such as synthetic porphyrins and phthalocyanines [2], corroles [3] and porphyrazines [4]. The exact mechanism of the natural reactivity and of many of the practical applications for synthetic porphyrinoids is often poorly understood, but the heteroaromatic nature of the porphyrinoid ligand is known to be a key factor.

The intense $\pi \rightarrow \pi^*$ absorption bands of magnesium chlorins are directly connected with the key role of plants in light harvesting within photosynthesis [5], while iron hemes carry out a wide range of chemistry moderated by the presence of the aromatic π-system [6]. In both cases, the brilliant colors and color changes in the UV–vis region of the spectrum have provided critically important insights into the electronic structures of these compounds. In the mid-1960s and early 1970s, magnetic circular dichroism (MCD) spectroscopy [7] provided the key to understanding the optical spectrum of porphyrinoids by confirming the validity of theoretical models [8–12] that had been developed based on molecular orbital (MO) theory to account for the relative intensities and wavelengths of the major spectral bands of chlorophylls, heme proteins and other porphyrinoids based on the orbital angular momentum (OAM) and magnetic quantum number (M_L) properties of the LUMOs and HOMOs of the porphyrinoid π-system. In the case of biologically significant transition metal porphyrinoid complexes such as the heme proteins [6], MCD spectroscopy also provided key information about the redox and spin state of the central metal, the redox state of the π-system and spectral band polarization information, which could not easily be derived from analysis of UV–vis absorption spectra and theoretical calculations, alone.

Despite these many key early successes, the MCD technique has not been universally adopted within the field of porphyrin and phthalocyanine research and MCD results are sometimes completely overlooked by researchers active within the field. A lack of familiarity with the theory on which the technique is based probably accounts for this, since it is seldom taught at the undergraduate level as part of courses on molecular spectroscopy. Conceptually, however, MCD spectroscopy should be readily accessible to anyone familiar with the theory of NMR and EPR spectroscopy and with introductory undergraduate level quantum mechanics.

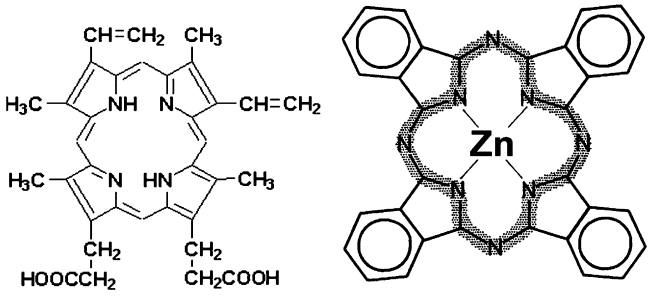

Fig. 1. Structures of protoporphyrin IX, the substituted porphin ligand that ligates iron in heme proteins (left), and a synthetic metal phthalocyanine complex (right).

The aim of this review is to provide key background knowledge for the general audience of porphyrinoid researchers to allow them to be able to interpret and assess the significance of MCD spectral data as readily as they would NMR or EPR data. A key conceptual problem in the application of MCD spectroscopy is that the analysis rests upon a molecular orbital (MO) approach to bonding, while the valence bond (VB) approach remains prevalent within both organic and inorganic chemistry at the undergraduate level and is still sometimes used within metal porphyrinoid research [13]. We, therefore, include a brief overview of the application of MO theory to aromatic and heteroaromatic π-systems required to fully appreciate the role of the orbital and spin magnetic quantum numbers within optical spectroscopy, before examining in detail several key applications of MCD spectroscopy within porphyrinoid research.

2. Theoretical background to MCD spectroscopy

2.1. Magnetism and optical spectroscopy

The major difference between MCD spectroscopy and the NMR and EPR techniques is that MCD spectroscopy is not based on resonance between spin states, but is instead based on the wavelength dependent absorption of circularly polarized light to form excited electronic states. The UV–vis absorption and MCD spectra of a molecular complex contain the same set of spectral bands, but the band morphologies are different due to the effect of the applied magnetic field and the use of a differential absorbance intensity scale from the CD spectrometer used for the measurements.

Five electronic quantum numbers [14] form the theoretical basis for magnetic circular dichroism since the interaction of electronic states with an applied magnetic field is based upon magnetic dipole moments associated with the orbital and spin motion of the electrons. The principal quantum number, n, was first proposed by Niels–Bohr to account for the wave based properties of electron orbital motion. Subsequently, during the process of solving the Schrödinger wave equation for hydrogen it was discovered that the OAM of the electron defined by the orbital quantum number, 1, is spatially quantized in terms of the z-component, L_z, defined by the magnetic quantum number, m_l, Fig. 2, based on precession at the Larmour frequency at fixed orientations around the axis of the applied magnetic field. In classical terms circular motion of charge in a current loop has a magnetic dipole based on the current (I) and the area (A) enclosed by the orbital motion:

$$\mu = IA = -\frac{e}{2m_e}L \tag{1}$$

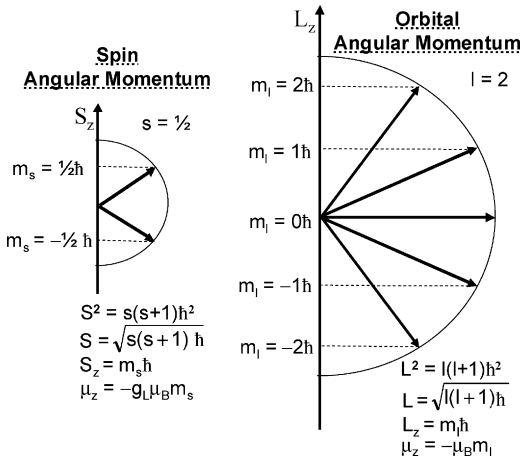

Fig. 2. The origin of the l, m_l, s and m_s quantum numbers and the associated magnetic moments.

When the quantized nature of OAM is factored in, the following equations can be derived:

$$\mu = -\frac{e}{2m_e}\sqrt{l(l+1)}\hbar = \sqrt{l(l+1)}\mu_B \quad (2)$$

$$\mu_z = -m_l\mu_B \quad (3)$$

where $l = 0, 1, \ldots, n-1$ and $m_l = 1, l-1, \ldots, 0, -l+1, -l$, e and m_e are the charge and mass of the electron, respectively, $\hbar$ is the Dirac constant ($h/2\pi$) and μ_B is the Bohr magneton. The negative sign arises since magnetism is defined in terms of a positive charge carrier and conventional current flow, which is still used by physicists for historical reasons.

In the case of spin angular momentum, the spin properties of an electron are quantized so that $s = 1/2$ and $m_s = \pm 1/2$, Fig. 2. Electron spin was found to be more efficient at producing a magnetic moment than the orbital motion so the magnetic moment equation for S_z contains the Landé factor (g-factor), which has a value of 2.0023:

$$\mu_z = -g_L m_s \mu_B \approx -\mu_B \quad (4)$$

We turn now to the incorporation of these atomic quantum number properties into the electronic description of a molecule. Predicting the optical spectrum requires the solution of the Schrödinger wave equation in terms of the states (Ψ_A) and energy levels (E_A) of the system and the Hamiltonian (H):

$$H\Psi_A = E_A\Psi_A \quad (5)$$

since this allows calculation of the observables transition energy and the oscillator strengths of the transition dipole moment between states A and J:

$$M^{AJ} = \langle \Psi_A | m | \Psi_J \rangle \quad (6)$$

Analysis of optical spectral data rests on the fact that absorption or emission of a photon of light with specific wavelength properties results in a redistribution of charge within a molecule based on a transition moment which couples the ground and excited electronic states, resulting in a new stationary electronic state, Fig. 3. A linear displacement of charge induces an electric dipole transition moment, while a magnetic dipole transition moment is induced by any circular motion of electric charge.

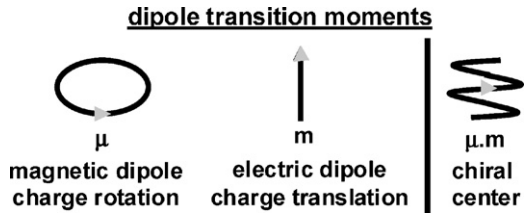

Fig. 3. The origin of chirality, based on the combined effect of electronic and magnetic transition moments.

Electric dipole moments (m) are the dominant factor in coupling the ground state with excited states within UV–vis absorption spectroscopy, since they tend to be ca. 5 orders of magnitude stronger than magnetic dipole moments (μ). In the case of dissymmetric molecules with a chiral center, however, absorption of a photon results in both magnetic and electric dipoles, since there is a helical redistribution of electronic charge. Enantiomers preferentially absorb left (lcp) and right (rcp) circularly polarized light based on the handedness of the helical electron redistribution. This differential absorbance of lcp or rcp forms the basis of circular dichroism (CD) spectroscopy [15]. Treatments of the selection rules for optical spectroscopy often focus primarily on whether a transition is spin ($\Delta S = 0$) forbidden and/or Laporte ($\Delta l = \pm 1$) forbidden, which in the case of centrosymmetric systems can also be expressed in terms of a change in parity such that $u \rightarrow u$ and $g \rightarrow g$ transitions are forbidden since s and d orbitals have gerade and p orbitals have ungerade nodal patterns. A third selection rule that only $\Delta M_L = 0, \pm 1$ transitions are fully allowed is often overlooked, since it is difficult to derive information based on this selection rule from standard UV–vis absorption spectra in the absence of an applied magnetic field which lifts the orbital and spin state degeneracies. We should note that this is a simplified account of optical selection rules which can be different under certain circumstances, in particular, there are additional rules concerning $L = 0$–0 and $M_L = 0$–0 transitions.

An incident photon can provide a maximum of one quantum of OAM ($\Delta M_L = \pm 1$), since the electric and magnetic vectors of the electromagnetic wave can rotate a maximum of once per wavelength, Fig. 4, and the total angular momentum within an

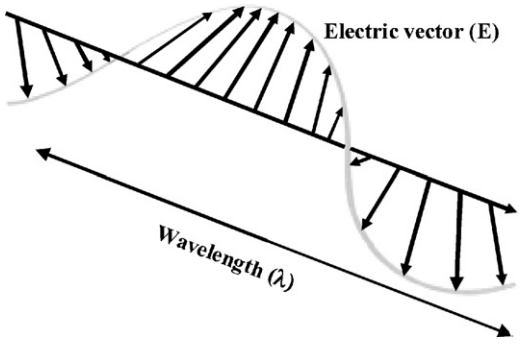

Fig. 4. The electric vector of lcp follows a counterclockwise path rotating once per wavelength along the axis of light propagation.

isolated system must be conserved in both magnitude and direction based on Newton's third law of motion. Absorption of a photon by a heteroaromatic π-system, such as that of a porphyrinoid ligand, results in both a linear and a circular redistribution of charge within the *xy*-plane, Fig. 3. Although strong magnetic dipoles are, therefore, induced within the $\pi\pi^*$ excited states of porphyrinoid π-systems, there is no net CD signal since in the absence of a chiral center the absorbance of lcp and rcp light is equally likely.

2.2. Zeeman splitting of states

The role of the magnetic vector of electromagnetic radiation tends to be neglected within optical spectroscopy with the exception of descriptions of line spectra arising from isolated atoms in the gas phase, and in astronomical observations. Within physical chemistry, this phenomenon is sometimes explained no further than the normal Zeeman effect observed during relaxation of an atomic hydrogen 1p orbital electron to the 1s orbital. The emission band is described as splitting into parallel (∥) and perpendicular (⊥) plane polarized bands, Fig. 5, based on $\Delta m_l = 0$ and $\Delta m_l = \pm 1$ selection rules, respectively, when the field lines are applied perpendicular to the emitted beam. What is seldom mentioned is that Pieter Zeeman's experiments (for which he shared the Nobel prize for physics in 1902 [16]) involved emission from a Cd 5d orbital to a 5p orbital with the magnetic field lines applied in both a parallel and a perpendicular arrangement relative to the axis of light propagation. In Zeeman's words during his Nobel prize lecture [16b] "...But let us first consider the rays which run parallel with the lines of force... The opposite circular oscillations of the electrons excite two circularly polarized rays rotating in opposite directions, one having a longer and the other a shorter period of oscillation than the original spectral line. The original spectral line splits up under the action of the magnetic field into two components which are circularly polarized in opposite directions. The light source emits two-color light...".

The MCD technique would probably be more widely appreciated if Zeeman's results were explained with greater emphasis placed on this ever first example of a magnetic circularly polarized emission spectrum. The MCD experiment in many respects is simply the reverse of Zeeman's observation in that differential absorbance of lcp and rcp photons is induced by the Zeeman splitting of states within an applied magnetic field.

Since cadmium has a closed shell d^{10} configuration, spin orbital angular momentum is not a factor in the normal Zeeman effect. When Zeeman studied metals with unpaired electrons such as sodium, however, multiple emission lines were observed both in the presence and absence of an external magnetic field. This is usually referred to as the anomalous Zeeman effect. In the case of sodium, a doublet is observed for the $3p \rightarrow 3s$ emission at zero field, since the electron spin angular momentum can either be aligned with or against the strong internal magnetic dipole created by the orbital motion of the unpaired electron. The anomalous Zeeman effect represents direct spectral evidence that spin and orbital angular momenta of the individual electrons couple to provide the total angular momentum quantum numbers, J and M_J, for the electronic state based on the L, M_L, S and M_s quantum numbers. In the case of the lighter atoms usually encountered in porphyrinoid research, including the first row transition metals ($Z < 40$), spin–orbit coupling is relatively weak and the L and S quantum numbers can be combined according to the Russell–Saunders coupling scheme (as opposed to the strong-field *j–j* coupling scheme observed in the case of heavier atoms where the spin–orbit coupling is stronger) to give the total angular momentum of the state J ($J = L + S$). When a magnetic field is applied, there is a lifting of state degeneracies into $2J + 1$ microstates based on the M_J quantum number for orientation relative to the applied field. The Zeeman splitting of the states, Fig. 6, can then be defined:

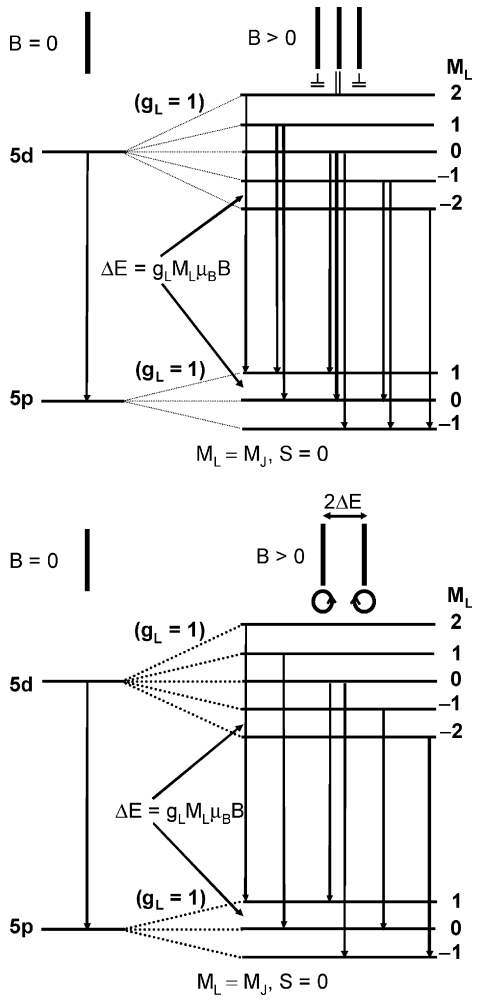

Fig. 5. The normal Zeeman effect. The emission from an atomic lamp source placed within a magnet observed perpendicular (top) and parallel (bottom) to the lines of force. It should be noted that when $S = 0$ and the Russell Saunders spin coupling mechanism is applicable, $J = L$, and $M_J = M_L$ as shown here.

$$\Delta E = \frac{e}{2m_e}(L_z + 2S_z)B = g_L \mu_B M_J B \tag{7}$$

The factor of 2 for S_z is related to g_L which was demonstrated empirically during early spectroscopic studies to be:

$$g_L = \frac{1 + J(J+1) + S(S+1) - L(L+1)}{2J(J+1)} \tag{8}$$

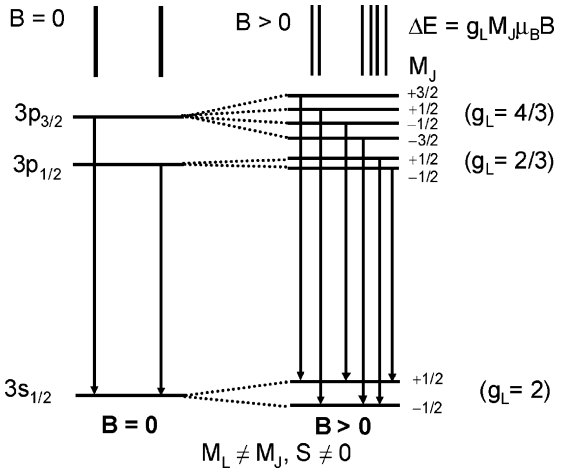

Fig. 6. The anomalous Zeeman effect. The emission from an atomic lamp source placed within a magnet observed parallel to the lines of force. Unlike the case in Fig. 5, J and M_J are now used since $S \neq 0$.

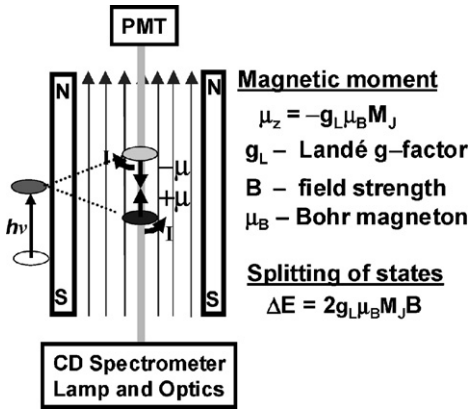

Fig. 7. The direction of the induced magnetic moments within a cyclic polyene excited state can be derived from Ampere's rule (right-hand rule) for a solenoid (i.e. for current in a loop). When the fingers of the right hand are curled in the flow direction for conventional current flow (i.e. for a positive charge carrier) the induced magnetic dipole moment is aligned in the direction the thumb is pointing. The MCD magnet's sample horizontal bore is surrounded by a solenoid to generate a high magnetic field, typically of 1–7 T, with field lines running from the south to north parallel to the axis of light propagation in the sample compartment of the CD spectrometer.

Since the g-factor associated with OAM, therefore, has a value of 1 when $S = 0$, this factor does not have to be included during the calculation of the Zeeman splittings of states for porphyrinoid complexes of diamagnetic main group and closed shell d^{10} metals.

The value for the z-component of the magnetic moment aligned with the axis of light propagation can be defined as

$$\mu_z = -\mu_B(L_z + 2S_z) \tag{9}$$

chiral lcp or rcp photon results in either a left or right handed redistribution of charge within the π-system, since the total OAM within the system must be conserved. The magnetic field lines induced by the circular redistribution of charge all point along the z-axis at the center of the ligand creating a magnetic dipole moment perpendicular to the plane of the π-system.

MCD spectra are recorded by mounting a magnet into the sample compartment of a CD spectrometer, in the Faraday alignment. Unlike EPR spectroscopy, even diamagnetic complexes exhibit an MCD signal. In the case of metal porphyrinoid $\pi \rightarrow \pi^*$ bands, absorption of a $\pi \rightarrow \pi^*$ bands, absorption of a chiral lcp or rcp photon results in either a left or right handed redistribution of charge within the π-system, since the total orbital angular momentum within the system must be conserved. The magnetic field lines induced by the circular redistribution of charge all point along the z-axis at the center of the ligand creating a magnetic dipole moment perpendicular to the plane of the π-system.

Within the MCD experiment the splitting of the optically accessible microstates of an excited state is:

$$\Delta E = 2g_L\mu_B M_J B \tag{10}$$

The factor of 2 is based on the fact that the microstate accessed by a photon of one handedness will be stabilized due to an alignment of the magnetic dipole moment with the applied field, while that accessed by a photon of the opposing handedness will be destabilized since the magnetic dipole is aligned against the field, Fig. 7.

A parallel applied field is often referred to as the Faraday alignment, since it was the basis of Michael Faraday's experiments in the 1840s [17] in which plane polarized beams of light were found to be rotated during transmission through certain substances due to the differential absorbance of lcp and rcp light. Since a perpendicular applied field tended to be used within Zeeman spectroscopy [18] (i.e. excited state emission experiments) a perpendicular alignment is sometimes referred to as the Zeeman magnet arrangement. Prior to the emergence of MCD spectroscopy in the mid-1960s, with the development of Ti–Nb and Sn–Nb alloy superconducting magnet coils and the photoelastic modulators required to create an alternating beam of lcp and rcp light from plane polarized light, magnetic optical rotatory dispersion (MORD) spectroscopy, which is based on Faraday effect experiments with plane polarized light, was the primary electronic absorption based technique used to study magnetic optical activity. Although MORD and Zeeman spectroscopy are now largely obsolete, in the early 1960s MORD experiments demonstrated the potential utility of magnetic optical activity for studying porphyrins, phthalocyanines and heme proteins [19] and inorganic anions [20]. MCD and MORD spectra are related by Kramers–Kronig transforms in the same manner as CD and ORD spectra [21].

2.3. MCD intensity mechanism and the three Faraday terms

The modern theoretical background to MCD spectroscopy is largely due to Buckingham, Stephens and Schatz [7,22]. In contrast with natural CD, which is relatively rare, the Faraday effect is a property of all matter. For a fully allowed electronic transition using the rigid-shift, Born–Oppenheimer and Franck–Condon approximations, the MCD intensity equation, according to the modified conventions recommended by

Stephens et al. [7], is:

$$\frac{\Delta\mathcal{A}_{\mathrm{l-r}}}{E} = 152.5\,Bcl\left[\mathcal{A}_1\left(-\frac{\mathrm{d}f}{dE}\right)+\left(\mathcal{B}_0+\frac{C_0}{kT}\right)f\right] \quad (11)$$

$\Delta A_{\mathrm{l-r}}$ is the differential absorbance of lcp and rcp light, B the field strength, cl the product of the concentration (mol l^{-1}) and path length (cm), E represents the energy coordinate in cm^{-1} and is used here to signify that the expression is for the entire spectral band rather than for just one wavelength, while f is a normalized band shape function (normally a Gaussian-shaped curve). Analysis of MCD spectra based on Eq. (11) is based on an estimation of the magnitudes of the three Faraday terms, $\mathcal{A}_1$, $\mathcal{B}_0$ and $\mathcal{C}_0$, which were originally used within the interpretation of MORD spectra [20,23]. Information can be derived based on the Zeeman splitting of the absorption bands for lcp and rcp light, the field-induced mixing of zero-field states and the Zeeman splitting based ground state population adjustment, respectively.

The dipole strength of the absorption intensity [7b] in the absence of an applied field is:

$$\mathcal{D}_0 = \frac{3.062\times10^{-3}}{\nu_{\max}}\int \varepsilon\,\mathrm{d}\nu \approx \frac{\langle\mathrm{A}\rangle_0}{326.6\mathrm{cl}} = \frac{\langle\varepsilon\rangle_0}{326.6} \quad (12)$$

where $\mathcal{D}_0$ is expressed in $(\mathrm{Debye})^2$ units (D^2) [7b,24], $\nu_{\max}$ is the band center energy in cm^{-1} and $\langle\mathrm{A}\rangle_0$ is the zeroth moment of the intensity for the entire absorption band. The right hand side equation is valid for any symmetrical band shape. It is important to note that throughout this section energies are in cm^{-1} and field strengths are in Tesla (T). In practical terms absorption and MCD spectra are normally reported in terms of extinction coefficients ε ($\mathrm{M}^{-1}\,\mathrm{cm}^{-1}$) and $\Delta\varepsilon_{\mathrm{M}}$ ($\mathrm{M}^{-1}\,\mathrm{cm}^{-1}\,\mathrm{T}^{-1}$) based on Beer's Law.

The $\mathcal{A}_1$ term, Fig. 8, arises from the Zeeman splitting of an orbitally degenerate excited state. There is a highly distinctive first derivative band shape due to the separation of the individual band centers of the lcp and rcp light absorbing bands. A consideration of Eq. (8) makes it clear that the $\mathcal{A}_1$ term intensity is based on the relative magnitudes of the combined orbital (L_z) and spin (S_z) angular momenta of electrons within the ground and excited states, labeled as A and J, respectively:

$$\mathcal{A}_1 = -\frac{1}{d_{\mathrm{A}}}\sum\langle J|\mu_z|J\rangle - \langle A|\mu_z|A\rangle([m_{-1}^{\mathrm{AJ}}]^2 - [m_{+1}^{\mathrm{AJ}}]^2) \quad (13)$$

where $[m_{-1}^{\mathrm{AJ}}]$ and $[m_{+1}^{\mathrm{AJ}}]$ are the electric dipole matrix elements associated with the absorption of lcp and rcp light, respectively, while d_{A} relates to the degree of degeneracy of the excited states. Note that the sign convention for handedness used in the subscripts of the matrix elements is the opposite of that used in $\Delta A_{\mathrm{l-r}}$.

The Gaussian-shaped $\mathcal{B}_0$ term arises from second order effects based on the field induced mixing of the zero-field states via magnetic dipole transition moments. $\mathcal{B}_0$ terms completely dominate the MCD spectrum when there is no three-fold or higher rotation axis, since there are no orbitally degenerate states that can be split due to the Zeeman effect. $\mathcal{B}_0$ terms are also present in the spectra of high symmetry complexes but tend to be significantly less intense than $\mathcal{A}_1$ and $\mathcal{C}_0$ terms, since there is a dependence on the energy separation of states J and K (ΔE_{KJ}) mixed by the field. $\mathcal{B}_0$ term intensity, in the absence of significant field induced mixing between the ground and excited states, is:

$$\mathcal{B}_0 = \frac{2}{d_{\mathrm{A}}}\Re\mathrm{e}\sum\frac{\langle J|\mu_z|K\rangle}{\Delta E_{\mathrm{KJ}}}([m_{-1}^{\mathrm{AJ}}][m_{+1}^{\mathrm{KA}}] - [m_{+1}^{\mathrm{AJ}}][m_{-1}^{\mathrm{KA}}]) \quad (14)$$

When a structural modification results in a small, relative to the spectral band width, zero-field splitting of what would otherwise be an orbitally degenerate $\pi\pi^*$ excited state, the resulting derivative-shaped signal is often referred to as a pseudo-$\mathcal{A}_1$ term, Fig. 9.

The $\mathcal{C}_0$ term arises, Fig. 10, from the Boltzmann population distribution across a degenerate ground state and, therefore, shows a strong $1/kT$ temperature dependence, Eq. (11). At very low temperatures, a symmetric Gaussian-shaped Faraday $\mathcal{C}_0$ term is observed because only the lowest split state contributes to the MCD. Understandably, the intensity of this $\mathcal{C}_0$ term dominates the MCD spectrum at low temperatures. At temperatures above saturation point at which the lowest microstate exists with

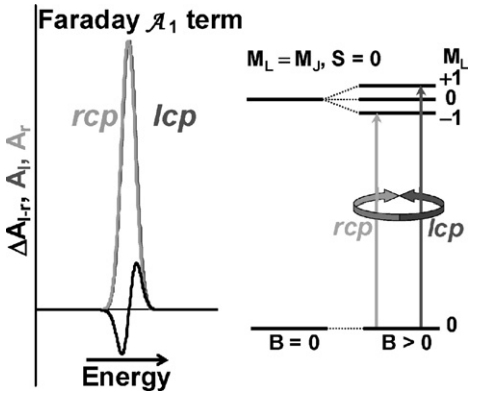

Fig. 8. Selection rules for the absorption of circularly polarized light based on a transition between an orbitally nondegenerate ground state and an orbitally degenerate excited state within a magnetic field applied parallel to the axis of light propagation. A derivative-shaped Faraday $\mathcal{A}_1$ term is observed due to the Zeeman splitting of states and the associated energy separation of bands absorbing lcp and rcp light based on the $\Delta M_{\mathrm{L}} = \pm1$ selection rule. We note that in this example, since $S = 0$ for closed shell atoms or molecules, $J = L$, and $M_{\mathrm{J}} = M_{\mathrm{J}}$.

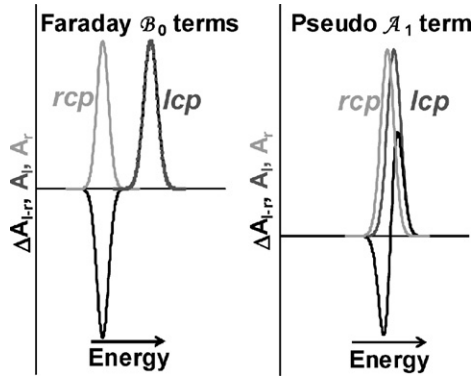

Fig. 9. The appearance and the intensity of coupled Faraday $\mathcal{B}_0$ terms depends upon the extent of the zero field splitting of states relative to the bandwidth. The splitting of the +ve and −ve Gaussian-shaped MCD signals (black) is determined by the energy separation of the lcp and rcp light absorption bands (dark and light gray) that arise within the applied field due to field induced mixing of states via a magnetic dipole transition moment.

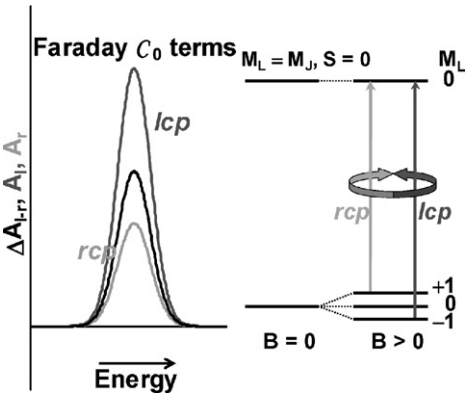

Fig. 10. Selection rules (right) for the absorption of circularly polarized light based on a transition between an orbitally degenerate ground state and an orbitally nondegenerate excited state within a magnetic field applied parallel to the axis of light propagation. $\mathcal{C}_0$ terms are extremely temperature sensitive. The $\mathcal{C}_0$ term has a $1/kT$ temperature dependence since the ground state microstates are populated according to a Boltzmann distribution. In this example $S = 0$ so $M_L = M_J$. The Faraday $\mathcal{C}_0$ terms which arise when $S \neq 0$ are described in Figs. 30 and 31.

100% of the population, the measured $\mathcal{C}_0$ term shape begins to become asymmetric due to the separation of the band centers of transitions absorbing lcp and rcp light, until both states are equally populated at very high temperatures at which point an $\mathcal{A}_1$-term-like derivative-shaped band will be observed. In the case of metal porphyrinoids, $\mathcal{C}_0$ terms are usually associated with the presence of an open shell transition metal. When the splitting of the microstates is small relative to the spectral bandwidths of the lcp and rcp light-specific absorption bands the $\mathcal{C}_0$ term is essentially Gaussian-shaped. $\mathcal{B}_0$ terms can be readily distinguished from $\mathcal{B}_0$ terms by measuring spectra at both room and cryogenic temperatures since they lack a $1/kT$ temperature dependence:

$$\mathcal{C}_0 = -\frac{1}{d_A}\sum \langle A|\mu_z|A\rangle([m_{-1}^{AJ}]^2 - [m_{+1}^{AJ}]^2). \tag{15}$$

2.4. Quantitative analysis of ground state and excited state magnetic dipoles

Comparison of Eqs. (13)–(15) for $\mathcal{A}_1, \mathcal{B}_0, \mathcal{C}_0$ with Eq. (16) for the dipole strength of the absorption band, $\mathcal{D}_0$, demonstrates that the electric dipole contribution is cancelled out within $\mathcal{A}_0/\mathcal{D}_0$, $\mathcal{B}_0/\mathcal{D}_0$, $\mathcal{C}_0/\mathcal{D}_0$ ratios:

$$\mathcal{D}_0 = \frac{1}{d_A}\sum [m_{\pm 1}^{AJ}]^2 \tag{16}$$

Since $\mathcal{D}_0$ can be readily derived from the corresponding UV–vis absorption spectra using Eq. (12), the MCD technique can be used to directly quantify the magnetic moments associated with the ground and excited states [7]. Method of moments analysis was introduced to MCD spectroscopy by Henry et al. [24] and has since been used extensively to derive the magnetic moments of the ground and/or excited states from MCD spectral data.

Unfortunately, several different sets of equations have been published for the moments of the three Faraday terms and Eqs. (11)–(15) which were recommended by Stephens [7a] and Piepho and Schatz [7b] in the late 1970s and which we regard as being the standard set of definitions within the field have not been universally adopted by all of the research groups active in the field of MCD spectroscopy. An earlier set of definitions for the three Faraday terms, which were adopted in the mid-1960s [25], usually denoted by $\boldsymbol{A}$, $\boldsymbol{B}$ and $\boldsymbol{C}$, have also been used extensively. The $\boldsymbol{A}$, $\boldsymbol{B}$ and $\boldsymbol{C}$ definitions were originally derived in the 1930s within the calculation of the Verdet constant, which is a measure of the wavelength dependent rotation of a plane polarized light beam in MORD experiments [20,23], while more recent sets of definitions, denoted as $\mathcal{A}_1$, $\mathcal{B}_0$ and $\mathcal{C}_0$, and $\mathcal{A}_1$(OLD), $\mathcal{B}_0$(OLD), $\mathcal{C}_0$(OLD) were developed specifically for use with MCD spectroscopy (see Section 2.5). The $\mathcal{A}_0$(OLD), $\mathcal{B}_0$(OLD), $\mathcal{C}_0$(OLD) and $\mathcal{D}_0$(OLD) definitions were used briefly by Stephens in the early 1970s [28]. The $\boldsymbol{A}$, $\boldsymbol{B}$, $\boldsymbol{C}$, and $\boldsymbol{D}$ and $\mathcal{A}_1$(OLD), $\mathcal{B}_0$(OLD), $\mathcal{C}_0$(OLD) and $\mathcal{D}_0$(OLD) definitions can still be found in recent MCD papers [26,27]. Within any review of the MCD literature the conventions used, therefore, need to be carefully checked. The conversion factors to derive $\mathcal{A}_1$, $\mathcal{B}_0$ and $\mathcal{C}_0$ values from the older definition are:

$$\mathcal{A}_1 = -\frac{2}{3}\mathcal{A}_1(\mathrm{OLD}) = \frac{2}{3}\boldsymbol{A} \tag{17}$$

$$\mathcal{B}_0 = -\frac{2}{3}\mathcal{B}_0(\mathrm{OLD}) = -\frac{2}{3}\boldsymbol{B} \tag{18}$$

$$\mathcal{C}_0 = -\frac{2}{3}\mathcal{C}_0(\mathrm{OLD}) = -\frac{2}{3}\boldsymbol{C} \tag{19}$$

$$\mathcal{D}_0 = \frac{1}{3}\mathcal{D}_0(\mathrm{OLD}) = \frac{1}{3}\boldsymbol{D} \tag{20}$$

A set of conversion factors quoted by Piepho and Schatz [7b] has caused considerable confusion for experimentalists. An extra factor of $1/\mu_B$ was included, which while technically correct in terms of their starting equations is not applicable for $\mathcal{A}_1$, $\mathcal{B}_0$, $\mathcal{C}_0$ and $\mathcal{D}_0$ values derived from observed ΔA and A values on the basis of Eqs. (11) and (12), since μ_B is already included within $\mathcal{A}_1/\mathcal{D}_0$, $\mathcal{B}_0/\mathcal{D}_0$ and $\mathcal{C}_0/\mathcal{D}_0$ ratio calculations as a factor of 152.5/326.6. The units for $\mathcal{A}_1$, $\mathcal{B}_0$, $\mathcal{C}_0$ derived from a direct application of these equations to experimental spectral data are $D^2\beta$ for $\mathcal{A}_1$ and D^2 cm β for $\mathcal{B}_0$ and $\mathcal{C}_0$, therefore, as was the case previously with $\boldsymbol{A}$, $\boldsymbol{B}$ and $\boldsymbol{C}$.

The factor of 2 in Eqs. (17)–(19) ensures that the z-component of the magnetic dipole moment for the ground and excited states can be derived directly from the $\mathcal{A}_1/\mathcal{D}_0$ and $\mathcal{C}_0/\mathcal{D}_0$ ratio values in instances where $S = 0$ and $g_L = 1$:

$$\mu_z\,(\text{excited state}) = -\frac{A_1}{D_0}, \qquad \mu_z\,(\text{ground state}) = \frac{C_0}{D_0} \tag{21}$$

The factor of 1/3 is related to the presence or absence of orientational averaging which takes into account the fact that in solution, molecules are randomly oriented so that the molecular axis does not coincide with that of the applied field. In practical terms, although this can affect the magnitude of $\mathcal{A}_1$, $\mathcal{B}_0$, $\mathcal{C}_0$ and $\mathcal{D}_0$, it usually cancels out within $\mathcal{A}_1/\mathcal{D}_0$, $\mathcal{B}_0/\mathcal{D}_0$ and $\mathcal{C}_0/\mathcal{D}_0$ ratio calculations. Random orientation is sometimes denoted with overbars [7b]. It should be noted that the difference between

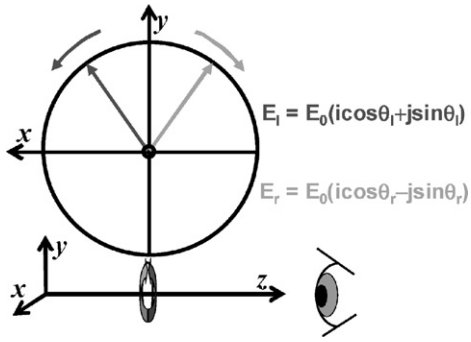

Fig. 11. The original definition of lcp and rcp within CD spectroscopy. Light plane polarized in the *yx*-plane can be described in mathematical terms as being comprised of left or right circularly polarized components of equal phase and amplitude (top). The towards the source perspective is depicted (bottom).

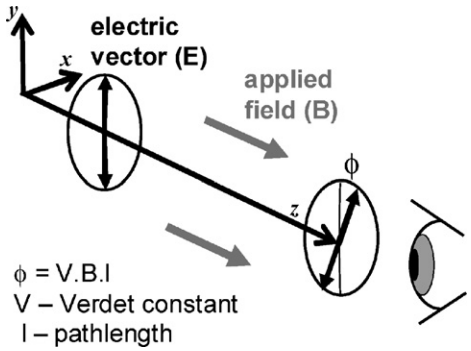

Fig. 12. The Faraday effect within MORD spectroscopy. A plane polarized beam is rotated by a magnetic field applied parallel to the axis of propagation. The rotation is defined as positive if the beam is rotated to the right in a clockwise direction when viewed towards the source.

randomly oriented solution spectra and spectra measured for a specific molecular orientation within a single crystal or argon matrices can potentially be a significant factor for complexes with anisotropic symmetries, and in those circumstances the equations required to analyze the Faraday terms may be significantly more complex than those included here, for example, manganese porphyrinoids complexes with E_g ground states [29].

2.5. Definitions of left- and right-handedness

One of the major problems faced in any description of magnetic optical activity is that differing left- and right-handedness conventions have been adopted depending on the context. The literature for MCD spectroscopy can be very confusing unless the reader firmly grasps that the classical optics definition used within CD and MCD spectroscopy is towards the light source with the axis of light propagation being defined by the *z*-axis, Fig. 11, as opposed to the perspective along the axis of light propagation normally favored by physicists. A clockwise right-handed perspective within one definition corresponds to a counterclockwise left-handed definition in the other.

Left handed photons were originally defined as positive since the electric vector rotates counterclockwise from the positive *y*-axis to the positive *x*-axis within a right-handed set of axes from positive *y*-values to positive *x*-values [13]. Unfortunately, the original definition for lcp light ($E_l = E_0(i\cos\theta_l + j\sin\theta_l)$) is the same as that used to define the right handedness of the α-helix of DNA [30] where the perspective is from the source along the axis of propagation. The application of CD spectroscopy has, therefore, been complicated in conceptual terms by the fact that left handed incident photons within the optical definition induce a right handed transition within the definition used for helical structures within proteins. The fact that the left- or right-handedness of a helix is independent of perspective when viewed from either end complicates matters further in conceptual terms; since it can provide the impression that handedness is completely independent of perspective.

Within MORD spectroscopy, Fig. 12, a positive Verdet constant and ϕ value for rotation of a plane polarized beam corresponds to clockwise right handed rotation when viewed towards the source. Absorption of incident lcp light, therefore, results in a positive signal within the CD intensity definition, but a negative Verdet constant based on negatively-signed component Faraday ***A***, ***B*** and/or ***C*** terms. Although MORD was developed first, MCD became the dominant technique since it is easier to derive values for $\mathcal{A}_1$, $\mathcal{B}_0$ and $\mathcal{C}_0$ from MCD spectra since there is greater resolution of the component spectral bands and there is no θ signal for the solvent and cell, which is a factor which had to be compensated for in MORD experiments [19a]. When the MORD definitions for the Faraday terms were initially adopted in MCD spectroscopy, this resulted in Gaussian-shaped MCD bands with a negative ΔA_{l-r} CD signal initially being referred to as positive ***B*** or ***C*** terms by researchers such as Michl [12] and Djerassi in key early papers on [25b]. Research groups who have subsequently adopted the modified moments definitions of Stephens [7a], Piepho and Schatz [7b] are now able to avoid this source of confusion and are able to refer to a negative ΔA_{l-r} signal as a negative Faraday $\mathcal{B}_0$ terms, since the sign of $\mathcal{B}_0$ matches that of ΔA_{l-r}. It should be noted, however, that the sign convention for the $\mathcal{A}_1$ term is the same as that of ***A***, since negative and positive ***A*** term terminology based on the high energy lobe of the derivative-shaped signal was well established and did not cause the same level of confusion as the Gaussian-shaped ***B*** and ***C*** term definitions. The $\mathcal{A}_1$(OLD) definition initially proposed by Stephens [28] was briefly the reverse of that of both the ***A*** term it replaced and the $\mathcal{A}_1$ term subsequently recommended by Stephens [7a] and Piepho and Schatz [7b], however.

An additional complication is that there are two different sets of units currently in widespread use to express MCD intensity. For historical reasons some research groups continue to use the field normalized, molar ellipticity unit $[\theta]_M$. Within the CD experiment, the incident plane polarized beam becomes elliptically polarized due to the differential absorbance of lcp and rcp light. While the ϕ unit in ORD spectroscopy is a measure of the rotation of the electric and magnetic vectors per unit field, concentration and distance, the θ unit in CD spectroscopy is defined in degrees based on the tangent of the ratio of the minor to major axes of the elliptical path followed by the electric vector within the *xy*-plane when viewed towards the light source. Initially the θ unit was adopted by CD spectroscopists so that results could be readily compared to MORD data via Kramers–Kronig transformations. Since θ is proportional to the differential absorbance of

lcp and rcp light, however, ΔA_{l-r} has increasingly been adopted and $\Delta\varepsilon_M$ based on the extinction coefficient for a 1 M solution at a field strength of 1 T is the preferred intensity unit for MCD spectroscopy. The conversion factors are $\theta = 32.98\Delta A$, where θ is expressed in units of mdeg or $[\theta]_M = 3.298\Delta\varepsilon_M$ where $[\theta]_M$ is expressed in units of deg cm^2 dmol^{-1}.

In summary in describing an MCD spectrum use the style, "positive $\mathcal{A}_1$ term" for a derivative-shaped signal that is negative to low energy of the cross-over point, and use "negative $\mathcal{B}_0$ term" and/or "negative $\mathcal{C}_0$ term" for Gaussian-shaped bands that have a negative ΔA_{l-r} signal based on Eqs. (11)–(16) using the modified conventions recommended by Stephens [7].

3. Overview of early research on the optical spectroscopy of porphyrinoids

3.1. Molecular orbital theory

One of the factors that can make MCD spectroscopy somewhat inaccessible to many organic and inorganic chemists is that either ligand field theory or a molecular orbital theory is required to interpret the spectral data. Although valence bond theory is still widely used as the conceptual framework for visualizing bonding and reactivity, an MO approach is required to account for the aromatic properties of benzene and other aromatic and heteroaromatic π-systems, such as the porphyrinoid π-system. Since the electron density for each molecular orbital is spread across the entire complex, the nodes and anti-nodes associated with the orbital angular motion around a π-system can be observed on the cyclic perimeters of aromatic molecules, Fig. 13. Linear combinations of the six carbon p_z orbitals which combine within the molecular orbital approach, result in three bonding and anti-bonding MOs with an $M_L = 0, \pm1, \pm2, 3$ sequence in ascending energy terms. The resonance energy of benzene, which accounts for the lack of reactivity, is based on the fact that all of the stabilized bonding MOs is fully occupied. This forms the basis of Hückel's $4N + 2$ rule for aromaticity.

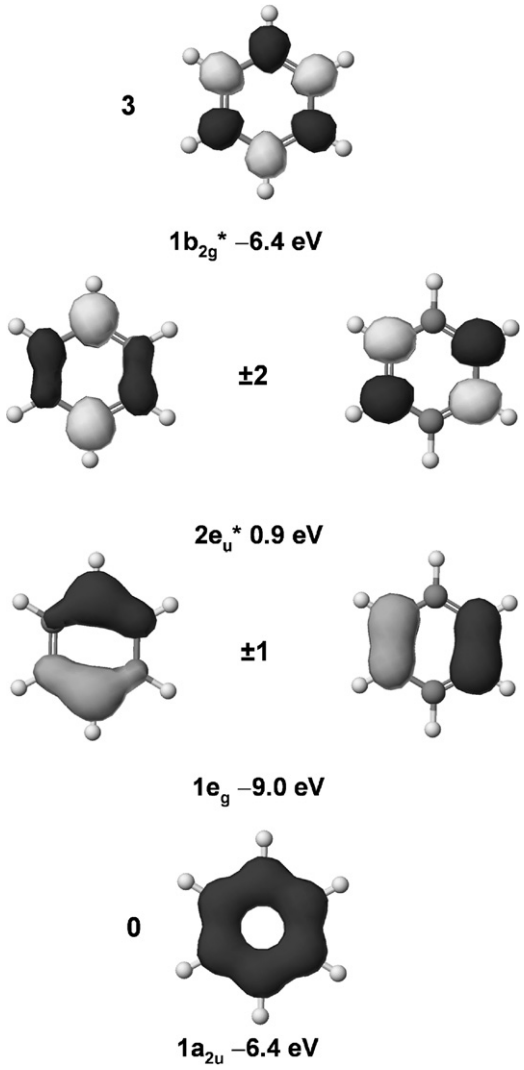

Fig. 13. The real MOs of benzene at an isosurface of 0.05 a.u. from the Tabulator program in the CAChe workstation software package [68] based on a DFT geometry optimization. Nodal patterns are observed on the inner cyclic perimeter, which arise from the magnetic quantum number properties associated with the corresponding complex wave functions, which have $M_L = 0, \pm1, \pm2$ and 3 OAM properties as shown.

3.2. Platt's free electron model for a cyclic π-system perimeter

In the late 1940s, Platt [9] proposed a free electron model for describing the energies of the π-system perimeter MOs in wavenumbers (cm^{-1}) based on an OAM quantum number (based on M_L) for the cyclic perimeter which was referred to as q:

$$E = \frac{q^2h^2}{2m_e l^2} \tag{22}$$

where m_e is the mass of the electron, h the Planck's constant and l is the length of the cyclic perimeter (Å). Since the HOMO and LUMO of benzene have $M_L = \pm1$ and ±2 nodal properties, respectively, Fig. 13, the $1e_{1g}$ and $1e^*_{2u}$ MOs can be viewed as being linked by an allowed $\Delta M_L = \pm1$ and a forbidden $\Delta M_L = \pm3$ transition, Fig. 14. Platt [9] referred to these as the B and L bands, respectively. The forbidden $\Delta M_L = \pm3$ transitions are located at lower energy based on Hund's second rule that for a given multiplicity the lower energy state has the greater angular momentum, Fig. 14. The B band is observed at 180 nm and is strongly allowed ($\varepsilon = 65{,}000$) with the L bands at 200 nm ($\varepsilon = 8000$) and at 254 nm ($\varepsilon = 254$) gaining intensity by vibrational borrowing.

3.3. LCAO based perimeter models

Moffitt [10] subsequently developed a more complex LCAO based model of the cyclic perimeter and noted the fact that in the case of cyclic heteroaromatic polyenes the nodal patterns for structural homologs based on the same basic ideal charged or uncharged parent C_nH_n perimeter are consistently retained and that the molecular orbital method used to predict the energies and relative intensities of the major spectral bands can be

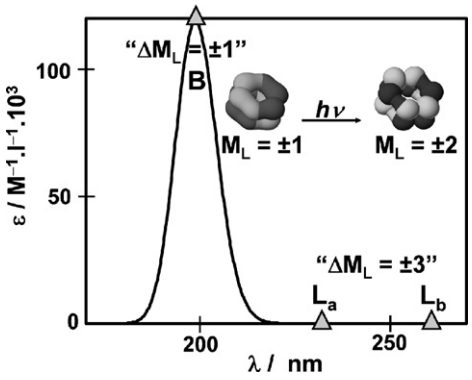

Fig. 14. Calculated UV–vis spectrum of benzene based on a DFT geometry optimization and INDO/s calculation performed using the CAChe workstation software package [68]. Triangles denote band centers associated with spin allowed electronic transitions. The B excited state is orbitally degenerate, $^1E_{1u}$. In contrast, the L excited states arising from the $\Delta M_L = \pm 3$ transition is nondegenerate with $^1B_{1u}$ and $^1B_{2u}$ symmetry in the case of benzene due to the D_{6th}, symmetry [9]. The L_a state is associated with nodes through the bonds, while the L_b state is associated with nodes through the atoms, Fig. 13.

simplified on this basis. A 16 atom 18 π-electron $C_{16}H_{16}^{2-}$ π-system, consistent with Hückel's $4N+2$ rule for aromaticity, can be viewed as being the parent cyclic perimeter of metal porphyrinoids based on the inner ligand perimeter. An $M_L = 0, \pm1, \pm2, \pm3, \pm4, \pm5, \pm6, \pm7$ and 8 sequence is observed in the molecular orbitals predicted on the basis on DFT optimizations of $C_{16}H_{16}^{2-}$ and zinc porphin. In the case of metal porphyrin complexes, the symmetry of the ligand is lowered from D_{16h} to D_{4h} due to the introduction of four pyrrole rings, but the same basic nodal pattern sequence can still clearly be observed within 16 of the 24π-MOs, Fig. 15, resulting in a similar calculated UV–vis spectrum, Fig. 16, to that obtained for benzene.

The basis of the perimeter model approach to the electronic structure of porphyrinoids is that although the original degenerate HOMO and LUMO orbitals, $1e_{4u}$ and $1e_{5g}^*$, may and do split in energy terms when the symmetry is lowered from the D_{16h} of $C_{16}H_{16}^{2-}$, these four frontier π-MOs still retain the $C_{16}H_{16}^{2-}$ nodal properties, which form the basis of the magnetic properties associated with the π-system which can be probed by MCD spectroscopy. The success of perimeter model based approaches, such as the research of Gouterman [11] and Michl [12], at interpreting the spectral properties of an extremely wide range of porphin-related compounds argues for this usage despite the fact that it is, of course, technically incorrect to speak of a split HOMO or LUMO. The focus of our attention is the explanation of the spectroscopic properties of porphyrinoids so we will use nomenclature such as ΔHOMO, and ΔLUMO that is well established within the literature of porphyrinoid spectroscopy [12], for the energy separation of the $1a_{1u}$ and $1a_{2u}$ top-filled MOs, which are derived from the $1e_{4u}$ HOMO of the parent $C_{16}H_{16}^{2-}$ hydrocarbon perimeter, with the proviso that we come to this description from a consideration of the HOMO and LUMO of the $C_{16}H_{16}^{2-}$ perimeter shown in Fig. 15 (left). Similarly, we will use the $1e_{5g}^*$ LUMO of the parent $C_{16}H_{16}^{2-}$ hydrocarbon perimeter.

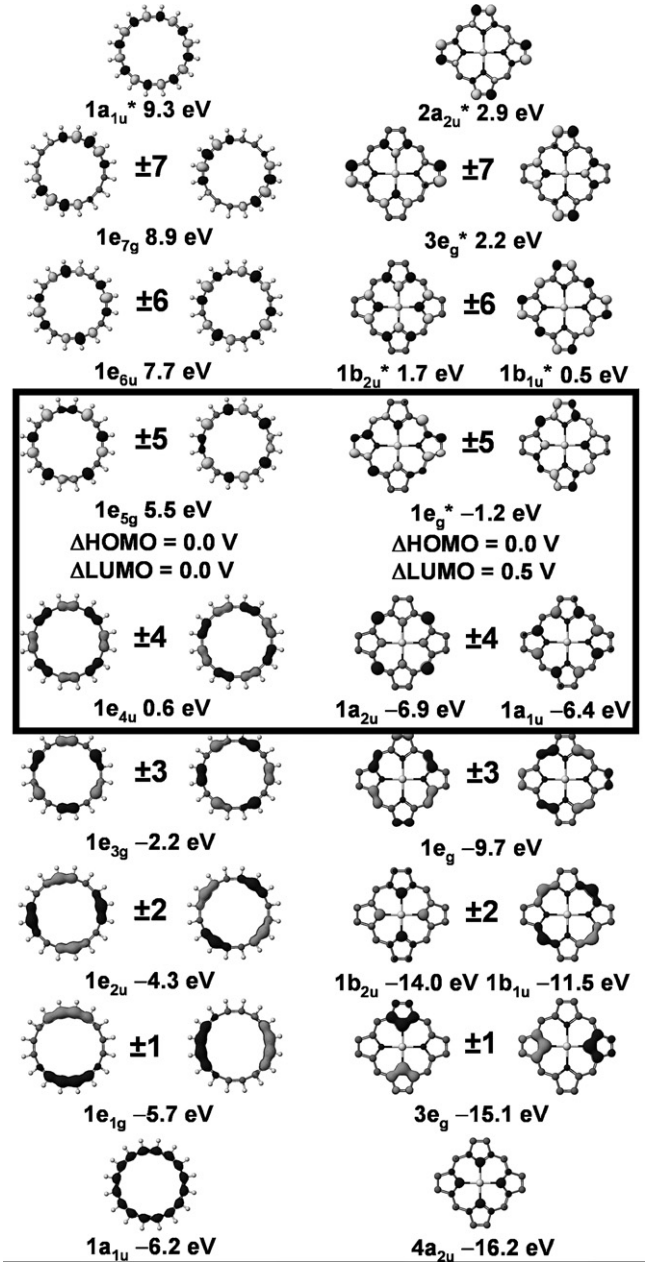

Fig. 15. The real π-MOs of the D_{16h} symmetry $C_{16}H_{16}^{2-}$ species (left) and the D_{4h} symmetry zinc porphin complex (right) at an isosurface of 0.05 a.u. from the Tabulator program in the CAChe workstation software package [68] based on a DFT geometry optimization. Nodal patterns can be observed on the inner cyclic perimeter based on the magnetic quantum number associated with the corresponding complex wavefunctions with $M_L = 0, \pm1, \pm2, \pm3, \pm4, \pm5, \pm6, \pm7$, 8 properties. The four frontier orbitals that form the basis of Gouterman 's four-orbital model and Michl's perimeter model are highlighted with black boxes. The ΔHOMO and ΔLUMO terminology used by Michl [12] relates to the perturbation of the frontier π-MOs relative to the $1e_{4u}$ and $1e_{5g}^*$ MOs of the $C_{16}H_{16}^{2-}$ parent hydrocarbon cyclic perimeter, respectively. It is convenient to use the ΔHOMO and ΔLUMO terminology because the UV–vis region spectroscopic properties of porphyrinoids can be understood in terms of the degree of symmetry-induced splitting of these nominally degenerate e_{4u} and e_{5g} molecular orbitals, vide infra.

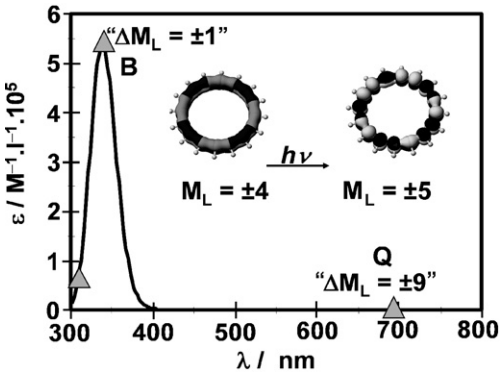

Fig. 16. Calculated UV–vis spectrum of a D_{16h} symmetry $C_{16}H_{16}^{2-}$ perimeter based on a DFT geometry optimization and an INDO/s calculation using the CAChe workstation software package [68]. Triangles denote band centers associated with spin allowed transitions. In the case of the $C_{16}H_{16}^{2-}$ perimeter the allowed and forbidden states are both orbitally degenerate with $^1E_{1u}$ and $^1E_{7u}$ symmetry [32], respectively. Michl refers to these bands as the B and L bands [12a].

3.4. Gouterman's four-orbital model

The spectra of synthetic main group metal porphyrins contain a fully allowed B band at ca. 400 nm (also referred to as the Soret band) and a set of weaker bands between 500 and 650 nm (arising from the forbidden $\Delta M_L = \pm 9$ transitions), Fig. 17. Early attempts at predicting porphyrinoid spectra based on a consideration of the entire 24 π-electron system within an LCAO approach proved problematic. Almost simultaneously with Platt's work on benzene, Simpson [8] proposed a free electron model based on an 18 atom 18 π-electron π-system in the case of free base porphyrin to account for the relative intensities of the bands within the absorption spectrum based on allowed and forbidden transitions with $\Delta M_L = \pm 1$ and ± 9 properties, respectively, Fig. 16.

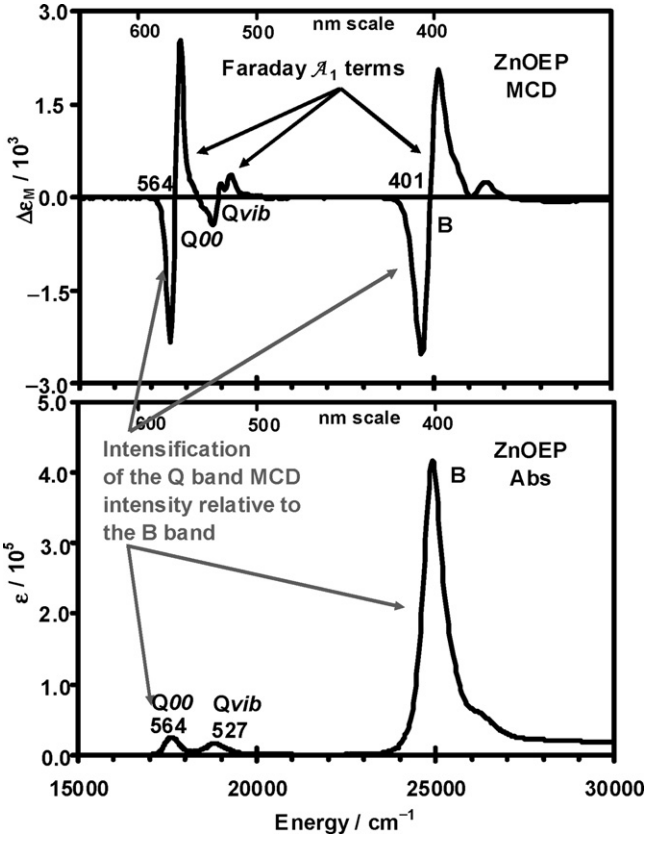

Fig. 17. Absorption and MCD spectra of zinc octaethylporphyrin (ZnOEP) in $CHCl_3$. Reproduced with permission from Ref. [39], copyright 2005 American Chemical Society.

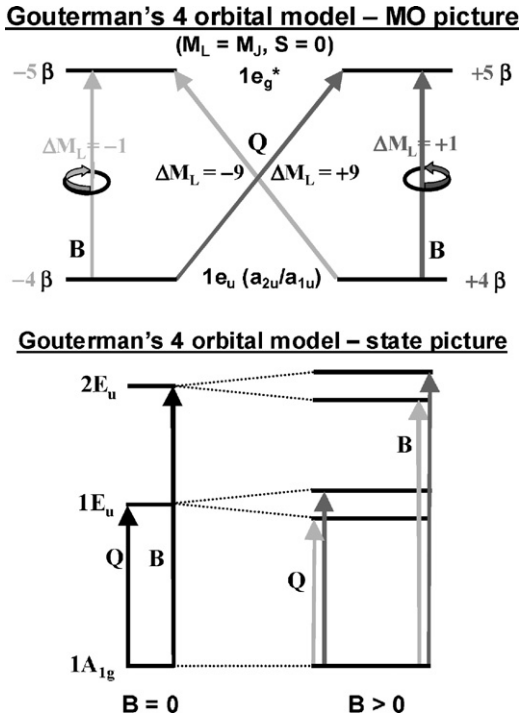

Fig. 18. Gouterman's four-orbital model [11] based on a consideration of only the HOMOs and LUMOs of the π-system (bottom). Reproduced with permission from Ref. [39], copyright 2005 American Chemical Society.

Gouterman subsequently developed a four-orbital LCAO model for porphyrinoid complexes in the 1960s, Fig. 18, after carrying out postgraduate research at Platt's laboratory at the University of Chicago [11a]. Gouterman's research [11] provided conclusive evidence that the weaker Q bands in the visible region were of $\pi\pi^*$ rather than $n\pi^*$ origins as some researchers [31] had suggested. The four-orbital model has since found widespread use as the conceptual framework to describe porphyrinoid optical spectra including those of the chlorophylls, proteins and a wide range of synthetic porphyrins and phthalocyanines [11]. Modern DFT techniques as well as the older semi-empirical methods such as PPP and INDO predict accidental degeneracy of the two π-system HOMOs, which would normally be expected to be nondegenerate under the D_{4h} symmetry typical for metal porphyrinoid complexes, Fig. 19. This forms the basis for understanding the spectroscopy of free base porphyrins and their metal complexes, since accidental degeneracy results in a spectrum with a set of electronically allowed ($\Delta M_L = \pm 1$) and forbidden ($\Delta M_L = \pm 9$) transitions between the HOMO and the LUMO based on the $\Delta M_L = \pm 1$ selection rule.

The forbidden band was referred to as the Q band in the case of porphyrinoids by Gouterman. Researchers within the porphyri-

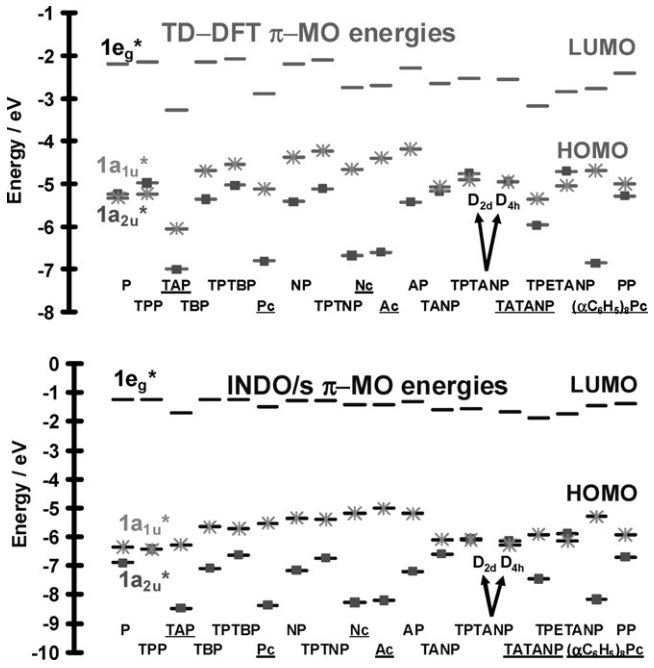

Fig. 19. Predicted energies of the four frontier MOs of 17 different zinc porphyrinoids, Fig. 28, derived from TD-DFT and semi-empirical INDO/s calculations based on B3LYP geometry optimizations with 6-31G(d) basis sets. Aza-substituted ligands such as Pc are underlined. Reproduced with permission from Ref. [39], copyright 2005 American Chemical Society.

noid field tend to be familiar with the Q and B band nomenclature from Gouterman's four-orbital model without being aware that the name for the Q band is based on the Japanese word for nine, kyuu, since $\Delta M_L = \pm 9$ character (when considered in simplistic free electron model terms) accounts for the electronically forbidden nature of the lowest energy electronic transition. The first use of the Q band terminology was by Platt [9b] who drew a distinction between bands associated with forbidden low energy transitions associated with orbitally degenerate excited states with $\Delta M_L > 1$ and the L_a and L_b bands observed in the case of benzene, Fig. 14, which are associated with nondegenerate excited states. This terminology was not adopted by subsequent researchers within the field of aromaticity, such as Michl, however, who continued to use Platt's original B and L band nomenclature for all aromatic and heteroaromatic π-systems [12a].

In the case of reduced symmetry complexes, for example the chlorins and bacteriochlorins where there is reduction of the double bonds at the periphery of the π-system, the degeneracy of the LUMOs and/or the HOMOs is lifted resulting in significant Q band absorption in the visible region, since the configuration interaction between the Q and B excited states is modified so that both the Q and B bands have electronically allowed character. In Gouterman's words the four-orbital model explained both within an easily understood qualitative conceptual framework, as well as on a more quantitative semi-empirical LCAO approach, why "grass is green and blood is red" [11].

Gouterman [11] demonstrated the validity of the four-orbital approach through extended Hückel calculations for a series of porphyrin, phthalocyanine and tetraazaporphyrin complexes. The relative magnitudes of the magnetic moment values for the $\pi\pi^*$ excited states were verified based on the $\mathcal{A}_1/\mathcal{D}_0$ ratios of the Q and B bands of metal porphyrins [11c], Fig. 17. Ceulemans et al. [32] have reported an in depth study for zinc tetraphenylporphyrin (ZnTPP) and zinc octaethylporphyrin (ZnOEP) reporting $\mathcal{A}_1/\mathcal{D}_0$ values typically between 2 and 5 for the Q band and between 0.5 and 1 for the B band depending on the nature of the axial ligation. Earlier Djerassi and coworkers [33] had reported slightly higher values in the 2.9–5.9 range based on cryogenic temperature measurements in a study of the effects of five and six coordination in the case of MgOEP and ZnOEP [33]. Axial ligation can lower the symmetry from D_{4h} to C_{2v} introducing a zero-field splitting of the $\pi\pi^*$ excited states due to a lifting of the orbital degeneracy of the LUMO. MCD spectroscopy has, therefore, provided direct spectroscopic evidence that the π-system HOMOs are accidentally nearly degenerate, thus forming an ideal cyclic polyene system similar to that studied by Platt in the case of benzene [9]. The values derived for the magnetic moments of the excited states are significantly lower than the $\mu_z = -1$ and $\mu_z = -9$ values that would be anticipated based on a free electron model of Simpson and Platt [8,9]. LCAO models, such as Gouterman's D_{4h} symmetry four-orbital model for electronic structure of porphyrinoids and Michl's D_{16h} symmetry perimeter model [12], which was derived from the earlier cyclic polyene approach of Platt and Moffitt [9,10] (see below), clearly provide a more accurate description of the magnetic moments of metal porphyrinoid $\pi\pi^*$ excited states. In the case of metal phthalocyanine complexes, where the porphyrin ligand is modified through the addition of aza-nitrogens and peripheral fused benzene rings, Fig. 1, the OAM associated with electron circulation in the HOMO of main group metal phthalocyanine complexes is largely quenched due to a >2 eV splitting of the $1a_{1u}$ and $1a_{2u}$ MOs, which are derived from the $1e_{4u}$ HOMO of the parent $C_{16}H_{16}^{2-}$ hydrocarbon perimeter, Fig. 19. The fully allowed and forbidden magnetic dipole character of the Q and B band is, therefore, lost and all four one-electron transitions within Gouterman's four-orbital model [11] become electronically allowed. The absorption spectrum of MPc, Fig. 20, includes an intense Q band (ε ca. 300,000 L mol^{-1} cm^{-1}) at ca. 670 nm, followed by a series of weaker vibrational bands, Q_{vib}, and a broad envelope of overlapping bands in the B band region of the spectrum (250–400 nm) [34]. The Q band retains its large magnetic moment due to the OAM associated with the orbitally degenerate LUMO. $\mathcal{A}_1/\mathcal{D}_0$ ratios of between 1.5 and 4.0 [35] are typically observed for MgPc and ZnPc depending on the nature of the axial ligand. The Q band completely dominates the MCD spectrum of main group metal phthalocyanines primarily due to significant band broadening in the B band region, since the observed peak-to-trough intensity of Faraday $\mathcal{A}_1$ terms is inversely proportional to the bandwidth, Fig. 20.

4. Practical application of MCD spectroscopy within porphyrinoid research

Having introduced the theoretical basis for MCD spectroscopy and having also provided a brief background to the analysis of porphyrinoid optical spectra based on MO theory, the focus for the remainder of this review will be on five different

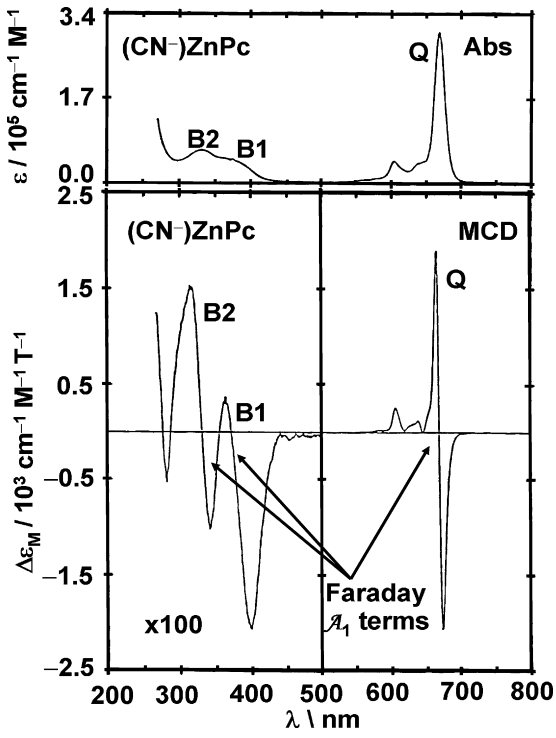

Fig. 20. Absorption and MCD spectra of (CN^-)ZnPc in dimethylacetamide. Reproduced with permission from Ref. [36c], copyright 1987 American Chemical Society.

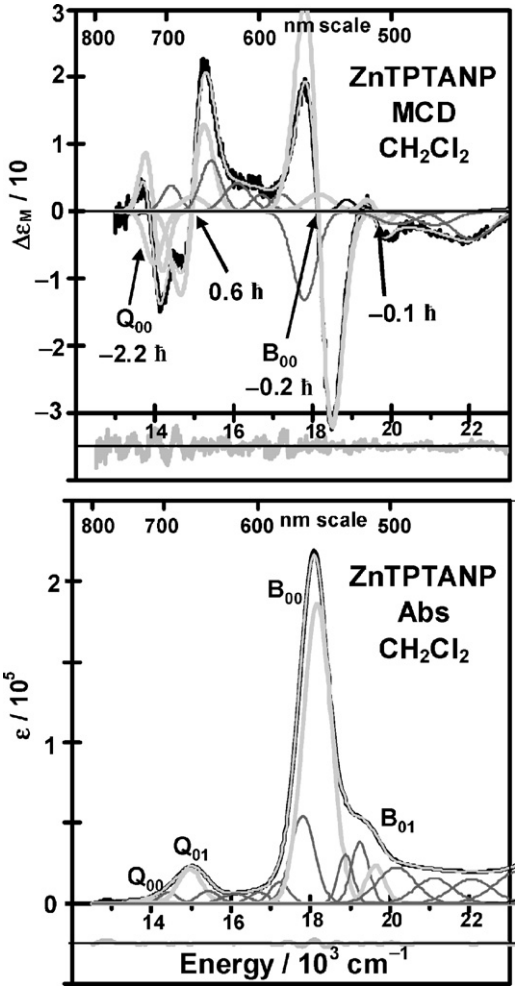

Fig. 21. Spectral deconvolution analyses of the absorption and MCD spectra of ZnTPTANP recorded in CH_2Cl_2. Reproduced with permission from Ref. [39], copyright 2005 American Chemical Society.

practical applications for MCD spectroscopy within porphyrinoid research: (i) the use of spectral band deconvolution analysis to identify the number of electronic transitions and to derive quantitative values for the three Faraday terms, (ii) the use of Michl's perimeter model, a general conceptual approach developed for aromatic and heteroaromatic π-systems based on the earlier work of Platt and Moffitt [9,10], which can be used to visualize the alignment of the induced $\pi\pi^*$ magnetic moments and to predict the sign sequences for the MCD bands arising from the Q and B, (iii) How MCD spectroscopy relates to the latest advances in molecular modeling software and in particular to the use of density functional theory (DFT) and how these calculations can be used in conjunction with Michl's perimeter model to predict $\mathcal{A}_1/\mathcal{D}_0$ ratios and μ_z values for $\pi\pi^*$ excited states, (iv) the use of MCD spectra recorded at cryogenic temperatures to derive information about orbital and/or spin degenerate ground states of transition metal complexes, and (v) the use of MCD spectroscopy as a complimentary method to EPR spectroscopy in studies of the electronic structure of paramagnetic anion and cation radical metal porphyrinoid species.

4.1. Spectral band deconvolution analysis

Method of moments analysis was the first approach used to derive $\mathcal{A}_1/\mathcal{D}_0$, $\mathcal{B}_0/\mathcal{D}_0$ and $\mathcal{C}_0/\mathcal{D}_0$ ratio values so that quantitative values could be derived for the ground and excited state magnetic moments. The technique is only suitable for baseline-to-baseline spectral band envelopes, however. Spectral deconvolution with Gaussian-shaped curves tends to be used to extract $\mathcal{A}_1/\mathcal{D}_0$, $\mathcal{B}_0/\mathcal{D}_0$ and $\mathcal{C}_0/\mathcal{D}_0$ ratios from spectral data sets that lack discrete baseline-to-baseline band envelopes [24]. The Stillman group have developed the Simpfit for Windows™ [37] spectral band deconvolution program, Fig. 21, to obtain the band energies and polarizations of the major spectral bands within the highly overlapping band envelopes often encountered in porphyrinoid UV–vis absorption and MCD spectral data using data recorded in optically transparent non-aqueous solvents at room and cryogenic temperatures [36]. Since the MCD and UV–vis absorption spectra arise from the same set of spectral bands, the measurement of a second data set removes much of the ambiguity normally associated with band deconvolution techniques. Under the rigid-shift approximation it can be assumed that the application of the applied magnetic field makes no difference to the spectral bandshape function.

Identifying the number of electronic origins within the UV–vis region can challenging when spectral bands overlap extensively. For example, Fig. 21, MCD spectroscopy identifies the electronic origin of the Q_{00} band within the optical spectrum of zinc tetraphenyltetraacenapthoporphyrin (ZnTPTANP), in what would otherwise appear to be a set of hot bands associated with the more intense Q_{01} vibrational band. In the case of

metal phthalocyanine complexes, spectral deconvolution studies by the Stillman group revealed that there are in fact two overlapping intense Faraday $\mathcal{A}_1$ terms of almost equal magnitude and bandwidth in the B band region, Fig. 20. This led to a modification of the Q, B, N, L and C band nomenclature [11e] originally proposed by Gouterman to include B1 and B2 band in the case of phthalocyanines [34]. This work has been reviewed recently elsewhere [34c,d] and will, therefore, not be covered here in detail. In recent years the Kobayashi and Stillman groups have extended the use of spectral band deconvolution beyond the initial focus on symmetric porphyrin and phthalocyanine ligands to a wide range of structurally modified porphyrinoids such as reduced symmetry π-systems, dimers and corroles [38,39].

4.2. Michl's perimeter model

Platt and Moffitt [9,10] were the first to develop a cyclic perimeter approach to the electronic structure of cyclic polyene systems and predicted the relative band intensities for the B and L bands based on the $\Delta M_L = 0, \pm 1$ selection rule. The nodal patterns of the frontier π-MOs are maintained even after substantial structural perturbations [12a] and can, therefore, be related back to those of an ideal high symmetry parent hydrocarbon. When a magnetic field is applied there is only very limited field induced mixing of the $\pi\pi^*$ states with $n\pi^*$ and $\sigma\pi^*$ states, so a perimeter model approach can also be used to study Faraday $\mathcal{A}_1$ or $\mathcal{B}_0$ terms within MCD spectra which arise from Platt's L and B transitions (i.e. the Q and B transitions within Gouterman's four-orbital model). In the 1970s, Michl [12] developed a general theory to account for the MCD spectroscopy of cyclic π-electron systems which could account in both qualitative and quantitative terms for the sign sequences of $\mathcal{A}_1$ (or of coupled oppositely-signed $\mathcal{B}_0$ terms in the case of lower symmetry complexes) based on a consideration of the excited state magnetic moments induced by the allowed and forbidden B and Q transitions within Gouterman's four-orbital model, Fig. 22. It was hoped that this would result in the MCD technique becoming a more widely used spectroscopic tool within organic chemistry. Michl's perimeter model [12] subsequently provided a key contribution to porphyrinoid research when Djerassi and coworkers used semi-empirical INDO/s based studies to predict the sign sequences observed for the chlorins, bacteriochlorins, isobacteriochlorins and monosubstituted free base porphyrins [40]. In recent years, Waluk, Sessler and coworkers [27] have used the perimeter model to study the electronic structure of porphycenes, dibenzoporphycenes, and smaragdyrins.

Since the π-system is based on the $2p_z$ atomic orbitals of the carbon atoms, complex wavefunctions for the cyclic perimeter permit a description of the net electron circulation upon electronic excitation based on the component atoms, which is not possible on the basis of the more commonly used real wavefunctions. A stack of MOs can be constructed for the 16 atom 18π-electron π-system on the inner ligand perimeter, Fig. 22. The magnetic moments for the 16π-MOs are plotted diagrammatically, based on the results of Michl's LCAO calculations, relative to the applied magnetic field. For each set of degenerate complex wavefunctions Ψ_N and Ψ_{-N}, the Ψ_{-N} MO involves

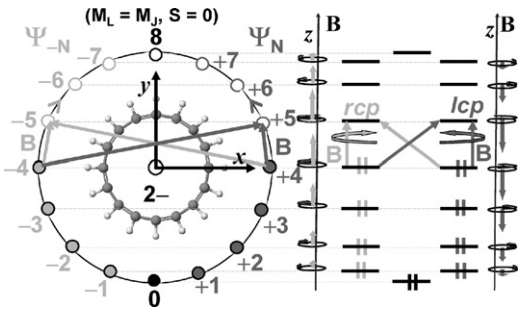

Fig. 22. Michl 's perimeter model (left) [12]. The circle is a diagrammatic representation of the clockwise and counterclockwise motion of π-system electrons on the $C_{16}H_{16}^{2-}$ parent perimeter of metal porphyrinoid complexes based on the 16 $2p_z$ atomic orbitals, generating the M_L value for each complex wavefunction MO. The perspective is towards the light source. The alignment of the magnetic moments within each MO generated with the applied field (right) can be predicted based on Ampere's rule (right-hand rule) for conventional current flow in a solenoid. The magnitudes are diagrammatic based on the result of INDO calculations [12]. Upon absorption of a photon of lcp or rcp, the excited electron typically retains the left or right handed motion on the perimeter associated with the M_L quantum number resulting in the electronically allowed B transition ($\Delta M_L = \pm 1$) so that the total angular momentum within the system is conserved. There is an electronically forbidden transition ($\Delta M_L = \pm 9$) named "L" in this context, which is associated with a reversal of the sense of electron motion on the perimeter (diagonal lines) and corresponds to the Q transition within Gouterman 's four-orbital model, Fig. 18.

electron circulation (based essentially on a redistribution of electronic charge from one $2p_z$ atomic orbital to another) in a clockwise direction from the lowest energy $M_L = 0$ MO, while the Ψ_N MO involves electron circulation in a counterclockwise direction.

When a magnetic field is applied parallel to the axis of light propagation, absorption of a photon of right or left circularly polarized light (lcp and rcp) results in either a $\Delta M_L = +1$ or a $\Delta M_L = -1$ transition as is the case in Zeeman's magnetic circularly polarized emission experiment [15], since the electric vector of the incident electromagnetic wave rotates clockwise or counterclockwise once per wavelength and the total angular momentum within the system must be conserved. This results in either clockwise or anticlockwise charge circulation on the inner ligand perimeter of the $\pi\pi^*$ excited state based on the direction of rotation of the electric vector of the incident photon, Fig. 22.

The alignment of the magnetic dipole induced within the excited state by this circular charge redistribution can be visualized based on Ampere's rule for current flow in a solenoid. When the fingers of the right hand are curled around the loop in the direction of conventional current flow (i.e. based on the charge carrier within the loop being positively charged), the thumb points in the direction of the dipole moment. A positive magnetic dipole moment, which points along the z-axis of the applied field is the energetically favored alignment within the Zeeman splitting of states. Since the perspective is towards the detector rather than the source, this corresponds to circulation induced within the cyclic perimeter of benzene by absorption of a photon of incident lcp [15].

In high symmetry cyclic polyenes, such as benzene, in which the π-MOs associated with the perimeter retain orbital degeneracy, Fig. 23, the OAM is no longer fully compensated for

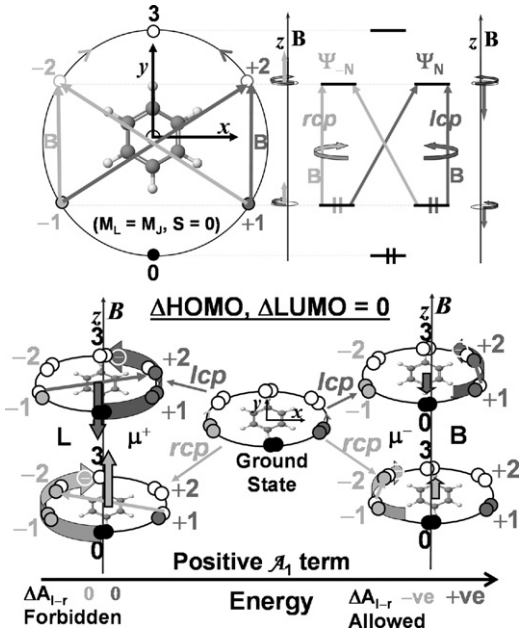

Fig. 23. The sign orderings of the positive $\mathcal{A}_1$ terms associated with Platt 's B and L bands [9] (top) is related to Ampere's rule (right-hand rule) for conventional current flow within a solenoid. When the fingers of the right hand are curled around the loop in the direction of conventional current flow (i.e. positive charge flow), the thumb is aligned with the magnetic dipole induced in the core of the current loop. The occupancy of the six complex MOs within Michl's perimeter model, Fig. 22, and the alignment of the μ^+ and μ^- magnetic dipoles, associated with the forbidden L and allowed B bands, induced through the absorption of a photon of either lcp or rcp are indicated with colored circles and arrows, respectively (bottom). The resulting MCD sign sequence in ascending energy terms is shown based on the Zeeman splitting of states which arises from the fact that a moment aligned with the applied field is energetically favored. The electronically forbidden L transition ($\Delta M_L = \pm 3$) corresponds to the Q transition within Gouterman 's four-orbital model for porphyrinoid π-systems, Fig. 18.

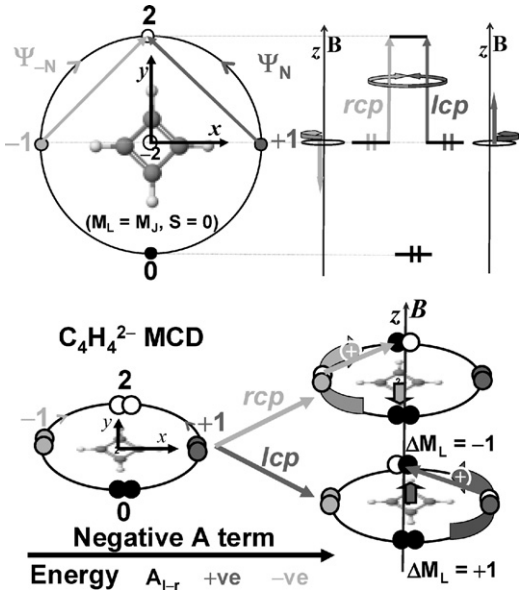

Fig. 24. The origin of negative Faraday $\mathcal{A}_1$ terms is based on a reversal in the alignment of the excited state magnetic dipoles induced by the Zeeman splittings of states. In an analogous manner to the $M_L = 0$ MO, the orbitally nondegenerate $M_L = 2$ MO has no net OAM, the lcp and rcp transitions, therefore, both obey the $\Delta M_L = \pm 1$ selection rule. The occupancy of the four complex MOs within Michl's perimeter model, Fig. 22, and the alignment of the magnetic dipoles induced through the absorption of a photon of either lcp or rcp are indicated with colored circles and arrows, respectively (bottom). The resulting MCD sign sequence in ascending energy terms is shown based on the fact that the moment aligned with the applied field is energetically favored.

by the motion of a second electron in the MO of the opposing handedness when an electron is promoted to the LUMO in an electric dipole allowed manner ($\Psi_N \rightarrow \Psi_{N+1}$ in the case of lcp and $\Psi_{-N} \rightarrow \Psi_{-N-1}$ in the case of rcp). When OAM is greater in the LUMO than in the HOMO, a negatively charged particle is effectively formed on the perimeter so the induced magnetic moment is aligned in the opposite direction from that generated by Ampere's Rule for solenoids based on conventional current flow and therefore results in a negative moment aligned against the field within the definition of handedness used by physicists and a positive Faraday $\mathcal{A}_1$ term, since the higher energy component has a positive ΔA_{l-r} signal in the MCD spectrum.

Positive Faraday $\mathcal{A}_1$ terms, Fig. 23, are the dominant spectral feature of high symmetry cyclic polyenes since the OAM associated with the LUMO is usually higher than that associated with the HOMO. The induced $\pi\pi^*$ magnetic moments for Platt's electronically allowed B and forbidden L transitions (which would have $\Delta M_L = \pm 1$ and $\Delta M_L = \pm 3$ properties in a free electron model approach) were referred to by Michl as the μ^- and μ^+, respectively. The μ^- magnetic moment is smaller in magnitude and less dependent on the structure of a complex since perimeters, while the μ^+ moment can vary greatly as a function of the number of atoms and electrons in the parent hydrocarbon perimeter and of perturbations to the electronic structure.

Kobayashi and coworkers [41] recently tested the validity of Michl's perimeter model [12] in a study of a four-atom six π-electron cyclobutadiene dianion. A negative Faraday $\mathcal{A}_1$ term was observed at 289 nm, as anticipated, for the $\Psi_{\pm 1} \rightarrow \Psi_2$ transition, Fig. 24. Since there is no OAM associated with the LUMO, the positive hole within the π-system HOMO as opposed to the negative charge within the LUMO is the dominant factor in charge circulation terms and the alignment of the magnetic dipole moments is reversed. The microstate associated with the absorption of lcp is therefore stabilized by the Zeeman splitting of states, so the negative lobe of the $\mathcal{A}_1$ term lies at higher energy.

When there is a minor zero-field splitting of the excited states due to a lifting of the orbital degeneracy of the HOMOs and/or the LUMOs, the $\mathcal{A}_1$ terms of high symmetry complexes are replaced by coupled oppositely signed $\mathcal{B}_0$ terms with the same basic −ve/+ve or +ve/−ve sign sequence. The Q and B transitions linking the frontier π-MOs of reduced symmetry porphyrinoids tend to have the strongest magnetic dipole transition moments and, therefore, are most extensively mixed by the applied field, Eq. (14). Michl successfully demonstrated that the alignment of the magnetic moment, Fig. 25, is determined by the relative energy separations of the frontier π-MOs derived from the $1e_{4u}$ HOMO and $1e^*_{5g}$ LUMO (ΔHOMO, ΔLUMO) [12a] of the $C_{16}H_{16}^{2-}$ parent hydrocarbon perimeter, Fig. 15. When $\Delta\text{HOMO} \gg \Delta\text{LUMO}$ the OAM associated with the excited electron predominates and there is a −ve/+ve/−ve/+ve ΔA_{l-r} intensity pattern with ascending

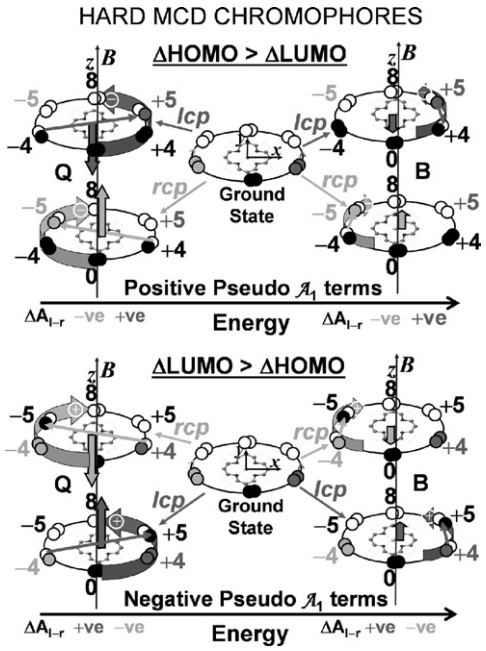

Fig. 25. The direction of the magnetic moments for the L and B bands of reduced symmetry porphyrinoids is determined by the relative energy separations of the frontier π-MOs derived from the $1e_{4u}$ HOMO and $1e^{*}_{5g}$ LUMO (ΔHOMO, ΔLUMO) [12a] of the $C_{16}H_{16}^{2-}$ parent hydrocarbon perimeter, Fig. 15, since this determines whether a positive or negative charge circulates on the π-system perimeter. Quenching of OAM properties of the electrons in either the HOMOs or LUMOs due to a structural perturbation, which introduces a large ΔHOMO or ΔLUMO, is denoted in black. Reproduced with permission from Ref. [39], copyright 2005 American Chemical Society.

energy for the Faraday $\mathcal{B}_0$ terms associated with Platt's L and B bands [9]. When ΔLUMO ≫ ΔHOMO circulation of the positive hole left within the HOMO becomes the predominant factor. The magnetic moments induced by the absorption of a photon of lcp and rcp light are reversed and the ΔA_{l-r} sign sequence for the Faraday $\mathcal{B}_0$ terms in ascending energy becomes +ve/−ve/+ve/−ve. It should be noted that Michl often used a reversed sign sequence based on the original MORD based definitions of the Faraday $\boldsymbol{B}$ term, which can cause considerable confusion.

The perimeter model is most useful for deriving structural information in the case of complexes with ΔHOMO ≈ ΔLUMO since small structural changes can reverse the direction of the induced magnetic dipoles excited state. Michl referred to these cyclic perimeters as soft MCD chromophores. We have recently reported a study of the MCD spectroscopy of ZnTPTANP [39] in which the Q and B bands appear as negative Faraday $\mathcal{A}_1$ terms with a +ve/−ve/+ve/−ve sign sequence in ascending energy, the sequence normally anticipated for a spectrum dominated by Faraday $\mathcal{B}_0$ based on a structural perturbations in which ΔLUMO > ΔHOMO. Non-planarity of the ligand due to steric hindrance appears to be the most likely explanation. The perimeter model is based on a consideration of only the electronic transitions, while vibrational bands can dominate the spectra of electronically forbidden transitions such as the Q band of ZnTPTANP, Fig. 21. In the case of perimeters in which ΔHOMO = ΔLUMO = 0, Michl [12] has pointed to the fact that in theoretical terms there is a −ve/−ve/−ve/+ve ΔA_{l-r} intensity pattern for the μ^{-} contribution to the Q and B bands. In practical terms, however, this is only of limited interest to the experimentalist since when the porphyrinoid Q band is formally forbidden it usually gains intensity from the B band through vibrational borrowing with an alternating positive and negative sequence being observed in the signs of the $\mathcal{A}_1$ terms for Q_{00}, Q_{01}, Q_{02} [42] as is the case with ZnTPTANP, Fig. 21. Michl theorized at length [12a] on how the perimeter model can be applied on a qualitative basis to predict the sign sequences of the MCD bands based on a consideration of the effect of structural perturbations to the ideal cyclic perimeter on the ΔHOMO and ΔLUMO of the four frontier π-MOs nodal patterns within the real wavefunctions. Recent advances in molecular modeling software have made a more quantitative approach to determining the relative magnitude of ΔHOMO and ΔLUMO more readily accessible than was the case in the late 1970s, however.

4.3. Density functional theory

Modern computational techniques such as DFT [43] can provide a significantly more accurate description of the ground state geometry than the semi-empirical techniques used by Gouterman and Michl in the 1960s and 1970s [11,12]. It should be noted, however, that commercially available DFT software packages are not fully *ab initio*, since they are based on exchange-correlation functionals such as B3LYP that are partially empirically derived. Calculated UV–vis spectra based on time-dependent DFT (TD-DFT) [44] should be treated with caution particularly when there is charge transfer between the ligand and the metal and the geometry of the excited states differs substantially from that of the ground state [45]. The application of DFT to transition metal porphyrinoid complexes remains highly problematic [46].

The main focus of the development of DFT within the field of optical spectroscopy has been on electric, rather than magnetic, dipole based properties. In 2003, the Gaussian software package [47] was upgraded to include predictions of CD spectra based on TD-DFT [48], however. Ziegler and coworkers [49] have recently reported DFT calculations of Faraday $\mathcal{A}_1$ terms of several inorganic anions and substituted benzenes based on the Amsterdam density functional program. $\mathcal{A}_1/\mathcal{D}_0$ ratios reported by Seth et al. are currently significantly lower than experimental values [49b] due to a neglect of environment effects on the incident radiation and the relatively low accuracy of dipole strengths calculated by TD-DFT.

Analysis of induced magnetic moments values derived from the three Faraday terms would represent an important additional spectroscopic basis for assessing the validity of DFT and TD-DFT based descriptions of the electronic structures and optical spectra of porphyrinoid complexes. Even in the case of the simplest porphyrinoid calculations based on metal porphins with a closed shell d^{10} central metal, the results of TD-DFT analyses cannot be accepted uncritically with a band assignment made by lining up the experimentally observed band wavelengths with those predicted by the calculation. It should be noted, for example, that two close lying intense *x*/*y*-polarized

$\pi \rightarrow \pi^*$ transitions of similar intensity were recently predicted in the B band region of zinc and magnesium porphin (ZnP and MgP) by Baerends et al. [50] based on statistical averaging of (model) orbital potentials (SAOP) calculations within the Amsterdam density functional package, Fig. 9, which appears to be inconsistent with the available MCD spectral data [11d], Fig. 17. We have observed similar results for the B band region of ZnTPP [39] based on TD-DFT calculations with the B3LYP functional of the Gaussian 03W software package [47] when using 6-31G(d) basis sets, but not in calculations with 6-31G basis sets or when using semi-empirical INDO/s calculations.

Despite the problems that can be encountered, the basic trends predicted for Q and B band intensity on the basis of the $\Delta M_L = 0, \pm 1$ the selection rule and semi-empirical calculations from Gouterman's four-orbital model and Michl's perimeter model, can be clearly observed in the results of DFT based calculations, Fig. 26. We recently reported a series of B3LYP and TD-DFT calculations for 17 radially symmetric zinc porphyrinoid complexes to study the effect of various structural perturbations on the wavelengths and intensities of the major bands in the UV–vis region. When the HOMOs are accidentally degenerate the Q transition is forbidden, Figs. 19 and 26, but when a large ΔHOMO is introduced the Q band gains significant intensity.

Despite the lack of calculated DFT based values for the three Faraday terms, it is still possible to estimate the magnitude of the induced magnetic moments for the Q and B excited states based on calculated oscillator strengths and values for μ^+ and μ^- calculated for the $C_{16}H_{16}^{2-}$ parent hydrocarbon of the inner ligand perimeter of porphyrinoid complexes [12a]. Michl reported tables for calculated μ^+ and μ^- moments of a wide range of possible parent hydrocarbon cyclic perimeters based on a set of $2p_z$ type Löwdin-orthogonalized atomic orbitals [51] and used Lindenberg's relation [52] to calculate PPP based electric and magnetic dipole operators with the ratio for the magnetic dipole matrix elements between next-nearest-neighboring Lowdin-AOs set as −0.15 MOs were calculated based on an ideal D_{nh} symmetry (where n is the number of atoms on the perimeter) with CI based on the four spin allowed one-electron transitions between the HOMOs and the LUMOs. The values obtained for a $C_{16}H_{16}^{2-}$ perimeter, were -0.01β and -6.24β, respectively. Michl derived the Eq. (23) for the electronic contributions to the Faraday $\boldsymbol{A}$ terms of the L and B transitions of a cyclic perimeter when ΔHOMO ≠ 0 and ΔLUMO = 0 in terms of the degree of mixing, α, in radians:

$$\frac{\mathcal{D}_0(\mathrm{Q})}{\mathcal{D}_0(\mathrm{B})} = \tan^2 \alpha \tag{23}$$

$$\mu(B) = \pm(\cos^2 \alpha)\mu^- \pm (\sin^2 \alpha)\mu^+ \tag{24}$$

$$\mu(Q) = \pm(\sin^2 \alpha)\mu^- \pm (\cos^2 \alpha)\mu^+ \tag{25}$$

The magnitude of the induced magnetic dipole moments of the Q and B excited states (μ(Q), μ(B)), Fig. 27, can be derived from the calculated oscillator strengths (f), Fig. 26, based on Eqs. (23)–(27), by converting the calculated oscillator strengths into dipole strengths based on Stephens, Piepho and Schatz's [7] modified convention for $\mathcal{D}_0$:

$$\mathcal{D}_0 = \frac{3.062 \times 10^{-3}}{\nu_{\max}} \int \varepsilon \, \mathrm{d}\nu \tag{26}$$

$$f = 4.319 \times 10^{-9} \int \varepsilon \, \mathrm{d}\nu \tag{27}$$

Values for μ(B) and μ(Q) were calculated, Fig. 27, on the basis of calculated Q band oscillator strength values from INDO/s and TD-DFT calculations for a set of DFT geometry

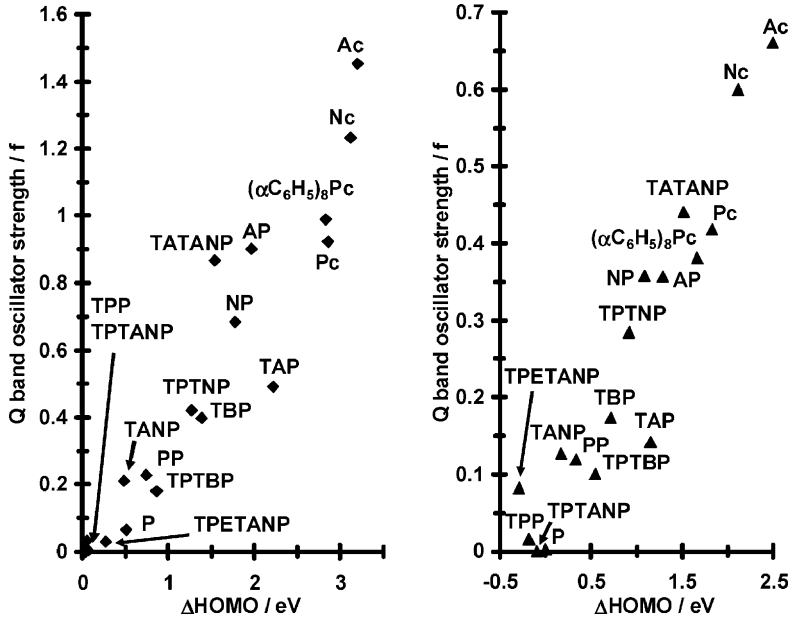

Fig. 26. Calculated Q band oscillator strengths of 17 Zn(II) complexes, Fig. 28, plotted against ΔHOMO from INDO/s (left) and TD-DFT (right) calculations based on B3LYP geometry optimizations with the 6-31G(d) basis set. Reproduced with permission from Ref. [39], copyright 2005 American Chemical Society.

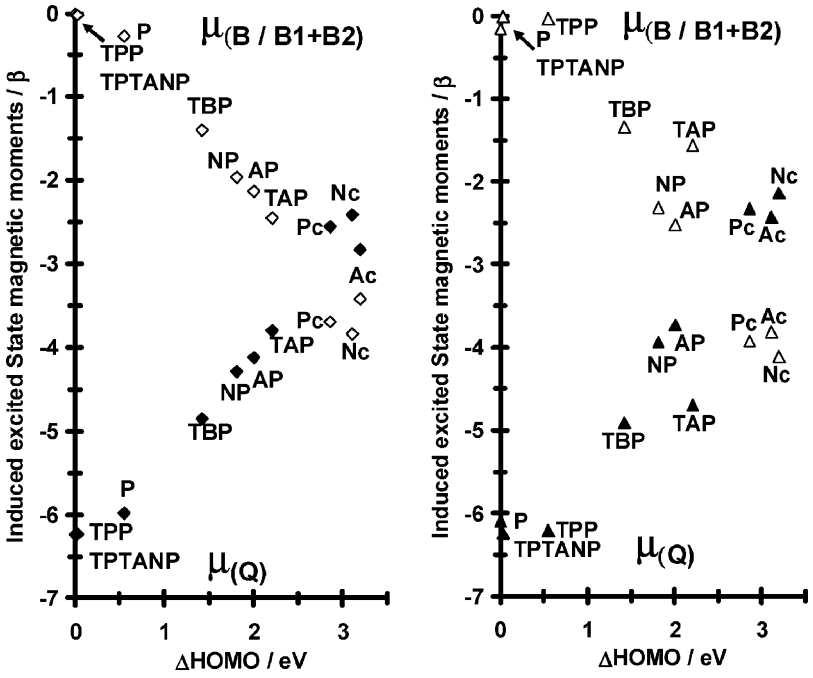

Fig. 27. The calculated excited state magnetic dipole moments for the Q and B bands (μ(Q), μ(B)) of 17 Zn(II) complexes, Fig. 28, plotted against ΔHOMO based on the oscillator strengths from INDO/s (left) and TD-DFT (right) calculations based on B3LYP geometry optimizations using the 6-31G(d) basis set. Closed symbols are used for μ(Q) and open symbols for μ(B). Reproduced with permission from Ref. [39], copyright 2005 American Chemical Society.

optimizations based on the B3LYP functional with 6-31G(d) basis sets. In the case of the parent perimeter, configuration interaction in the INDO/s calculations for the Q and B excited states is almost exclusively between the $1a_{1u} \rightarrow 1e_g^*$ and $1a_{2u} \rightarrow 1e_g^*$ one electron transitions, Fig. 18. When the Q band loses its fully forbidden character and gains significant absorption intensity due to a lifting of the degeneracy of the HOMOs, Fig. 20, there is significantly increased mixing between the B (or B1) and higher energy $\pi\pi^*$ states, Table 1, which often (particularly in the case of fused ring expanded and aza-substituted porphyrinoids (Fig. 28)) results in a much more complex optical spectrum within the UV region than that observed for porphyrin complexes, Fig. 17. Since the interaction with higher energy $\pi\pi^*$ states in the UV region is not included in the 4-orbital based perimeter model, Michl's approach is, therefore, best suited to predicting the sign sequence and moment observed for the Q bands of porphyrinoid ligands with high α values in Eq. (23) [39].

4.4. MCD spectroscopy of transition metal complexes

Since the mid-1960s, MCD spectroscopy has found considerable use in biochemistry for studying heme-proteins, such as myoglobin and hemoglobin [6], and other biologically significant transition metal complexes. The redox chemistry of transition metal porphyrinoid complexes is significantly more complex than that of main group metal and closed shell d^{10} metal complexes due to the partially filled d shell. MCD spectroscopy has consistently provided key ground and excited state degeneracy information that cannot easily be derived from analysis of UV–vis absorption spectra and theoretical calculations, alone. The MCD technique is complementary to EPR spectroscopy, which provides key information about the electron spin state of paramagnetic complexes. The complex band morphologies arising from the three Faraday terms result in major changes within the overall MCD spectrum. In contrast, only relatively minor

Table 1
The percentage contribution of the $1a_{1u} \rightarrow 1e_g^*$ and $1a_{2u} \rightarrow 1e_g^*$ transitions from Gouterman's four-orbital model to the Q and B/B1 bands based on eigenvector values from INDO/s calculations using B3LYP based geometry optimizations with 6-31G basis sets

	Q[a]	B/B1[a]	α (°)[b]	ΔHOMO[c] (eV)
$C_{16}H_{16}^{2-}$	49:49	49:49	0	0.00
P	63:34	33:60	12	0.50
TAP	85:12	8:64	39	2.22
TPP	51:46	45:49	0.4	0.03
TBP	78:19	19:72	29	1.38
Pc	91:6	22:55	50	2.86
TPTBP	70:27	26:67	19	0.86
NP	83:13	9:68	34	1.78
TPTNP	78:18	39:42	28	1.27
Nc	95:3	2:47	51	3.12
AP	85:9	4:45	36	1.97
Ac	92:2	2:25	48	3.20
TANP	65:28	23:52	18	0.48
TPTANP	55:40	37:51	0.4	0.07
TATANP	86:8	5:46	49	1.54
TPETANP	52:42	41:51	6.1	0.27
PP	71:23	22:59	20	0.74
$(\alpha C_6H_6)_8Pc$	92:5	4:45	60	2.83

[a] The percentage contribution of the $1a_{1u} \rightarrow 1e_g^*$ and $1a_{2u} \rightarrow 1e_g^*$ eigenvectors to the Q and B/B1.

[b] α, the degree of mixing of the magnetic properties of the Q and B/B1 excited states on the basis of Eqs. (23)–(25), Figs. 26 and 27.

[c] Energy separation (eV) of the MOs derived from the $1e_{4u}$ HOMO of the $C_{16}H_{16}^{2-}$ parent hydrocarbon perimeter.

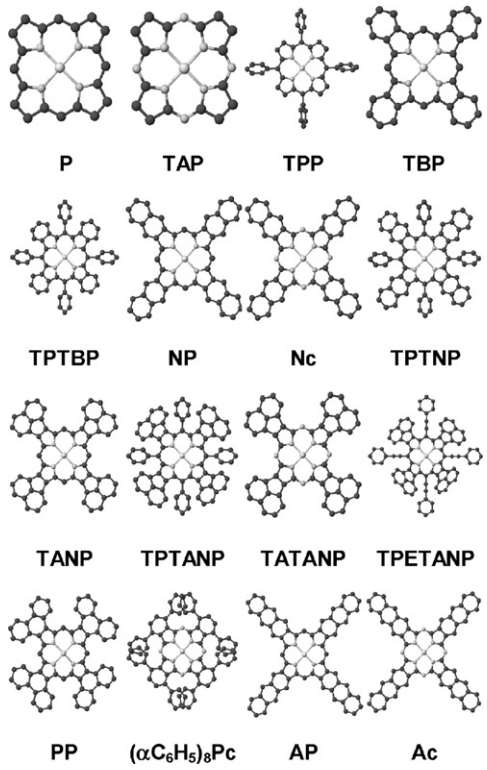

Fig. 28. Molecular structures of the zinc complexes of porphyrin (P), tetraaza- (TAP), tetraphenyl- (TPP), tetrabenzo- (TBP), tetraphenyltetrabenzo- (TPTBP) and naphtho- (NP) porphyrins, naphthalocyanine (Nc), tetraphenyl-tetranaphtho- (TPTNP), tetraacenaphtho- (TANP), tetraacenaphthotetraaza- (TATANP), tetraphenyl-tetraacenaphtho- (TPTANP), tetraphenylethynyl-acenaphtho- (TPETANP), tetraphenanthro- (PP) porphyrins, octa-α-phenylphthalocyanine ($(\alpha C_6H_5)_8Pc$), anthracoporphyrin (AP) and anthracocyanine (Ac) based on DFT geometry optimizations using the B3LYP functional of the Gaussian 03 program [47] with 6-31G basis sets. The structure of phthalocyanine (Pc) is shown in Fig. 1.

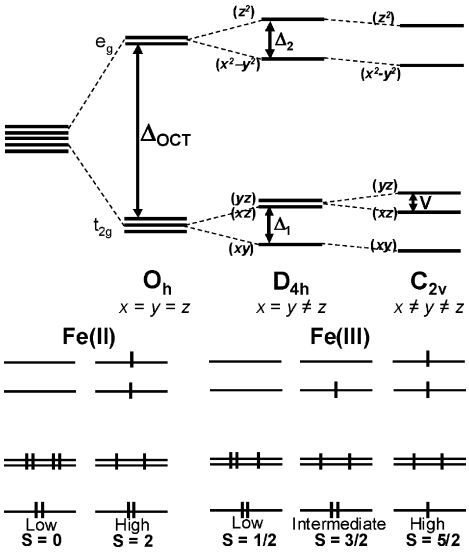

Fig. 29. The crystal field splitting of Fe(II) and Fe(III) d orbitals in cubic O_h, tetragonal D_{4h} and rhombic C_{2v} environments (TOP). Only the latter two are typically observed for metal porphyrinoid complexes. The axial and rhombic ligand field parameters are denoted as Δ and V. The low, intermediate and high spin states for Fe(II) and Fe(III) based on a tetragonal environment (bottom).

changes in band centers and intensities are typically observed in the UV–vis absorption spectra [2b,6, 11c, 36b,d].

Since there is a partially filled set of d orbitals, ligand to metal and metal to ligand charge transfer bands (LMCT, MLCT) bands are observed in both the absorption and MCD spectra in addition to the $\pi \rightarrow \pi^*$ bands. The ligand field splitting of the d orbitals in metal porphyrinoid complexes tends to be essentially tetragonal based on the tetradentate nature of the porphyrin ligand and some form of axial ligation from above and below the ring. In an O_h symmetry environment the ligand field splitting (Δ_{OCT}) is typically of the order of 10,000 cm^{-1}. Most six coordinate D_{4h} symmetry porphyrinoid complexes are axially distorted ($x = y \neq z$) so that the degeneracy of the e_g and t_{2g} levels is lifted, while lower symmetry porphyrinoids contain a rhombic distortion ($x \neq y \neq z$) in which there is a complete lifting of d orbital degeneracy. In the case of Fe(II) and Fe(III) complexes, the spin state of the central metal is determined by the nature of axial ligation from above and below the ring.

Strong ligands such as CO and CN^-, which act as π-acceptors based on back bonding, result in low spin complexes by increasing the separation of the e_g and t_{2g} orbitals, while weak ligands, which act as π-donors, such as F^- reduce the separation and result in a high spin state with $S > 1/2$. In the case of Fe(III) hemes, ligation with azide (N_3^-) can also result in an intermediate spin state with $S = 3/2$ [53]. In complexes where there are unpaired electrons so that $S > 0$, spin–orbit coupling, Fig. 29, results in zero-field splitting (ZFS) of state degeneracies in addition to the ligand field effects on orbital degeneracy, which are related to the axial and rhombic distortions to the coordination sphere of the central metal.

For example the low, intermediate and high spin states of Fe(II) and Fe(III) porphyrin complexes (e.g. in heme proteins) depend on the nature of axial ligation from above and below the ring with the configuration interaction between the main $\pi \rightarrow \pi^*$ and charge transfer states resulting in distinctive "fingerprint patterns" that can be used to derive information [6a,b], which can help to provide answers to a series of questions: (i) How many ligands are attached to the iron and what is the nature of these coordinating ligands (in the case of a protein, nitrogen from a histidine or a sulfur from a cysteine, for example)? (ii) Is the spin state of the iron high, intermediate or low, which relates to the binding strength of the axial ligand present. (iii) What is the oxidation state of the central iron (Fe(II), Fe(III) and Fe(IV))? (iv) Can the heme iron be readily oxidized or reduced? (v) And finally can axial ligands approach and bind to the iron? Recently the Stillman group have used this approach to explore the heme binding properties of iron-regulated surface determinant proteins in the human pathogen *Staphylococcus aureus* [54]. Dawson and coworkers have also recently reported MCD analyses of analogous Fe-containing proteins [55].

Key information about the ground state degeneracy can be derived by determining whether the MCD spectrum contains Faraday $\mathcal{C}_0$ terms with a $1/kT$ temperature dependence, Fig. 30. For example, in the case of Fe(II) and Ru(II) porphyrinoid MCD

spectra, the absence of temperature dependence is consistent with the presence of a low spin d^6 central metal configuration with $S=0$. For heme proteins, this configuration can normally be obtained through reduction with $Na_2S_2O_4$ and the addition of a strong axial ligand [6a]. The MCD spectra of low spin d^6 porphyrinoid complexes, such as $Fe^{II}Pc$ and $Ru^{II}Pc$ [34c,36d,36k], are dominated by Faraday $\mathcal{A}_1$ terms and are typically similar to those of main group metal and closed shell d^{10} Pc complexes, complicated somewhat by the presence of metal to ligand and ligand to metal charge transfer (MLCT and LMCT) in addition to the major main $\pi \rightarrow \pi^*$ transition observed for main group metal complexes.

In the case of Fe(III) hemes with d^5 central metal configurations, LMCT bands in the near IR (1000–2000 nm) are an ideal probe for determining the extent of rhombic splitting of the $d_{(yz)}$ and $d_{(xz)}$ orbitals, Fig. 29. Thomson [56] has reported combined EPR, MCD and UV–vis absorption spectroscopic studies which demonstrate that the near IR region LMCT bands for a series of low spin Fe(III) hemes can be used to determine the nature of the axial ligands as had earlier been reported by Stephens and coworkers based on MCD spectroscopy of cytochrome c at room temperature [57] and also by Hatano and coworkers based on measurements between 138 and 283 K [58].

Since $S=1/2$, the ground and excited states of low spin d^5 complexes will split into Kramer's doublets within an applied magnetic field with $M_S=-1/2$ and $M_S=+1/2$. At high temperature and low field, the lcp and rcp absorbing transitions result in spectral bands that tend to cancel resulting in a weak MCD signal, Fig. 30. As the temperature is lowered or the applied field is increased, the Boltzmann population of the higher sublevel decreases and the $\mathcal{C}_0$ term, therefore, increases in intensity. During measurement of vitreous solutions at cryogenic temperatures (1–4 K) and high field strengths (4–7 K), the lowest component of the ground state will often be populated and the MCD signal saturates.

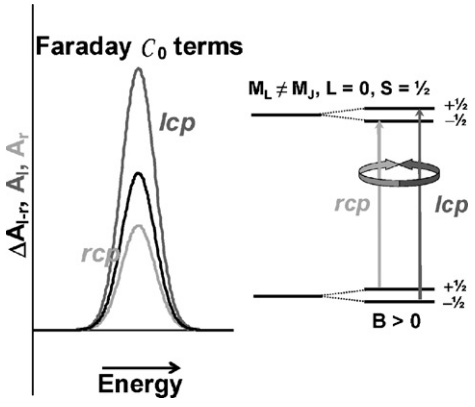

Fig. 30. Selection rules (right) for the absorption of circularly polarized light based on a transition between an orbitally degenerate ground state and an orbitally nondegenerate excited state within a magnetic field applied parallel to the axis of light propagation. A Gaussian-shaped Faraday $\mathcal{C}_0$ term is observed due to the separation of the band centers for the absorption of lcp and rcp light. The $\mathcal{C}_0$ term has a $1/kT$ temperature dependence since the ground state microstates are populated according to a Boltzmann distribution.

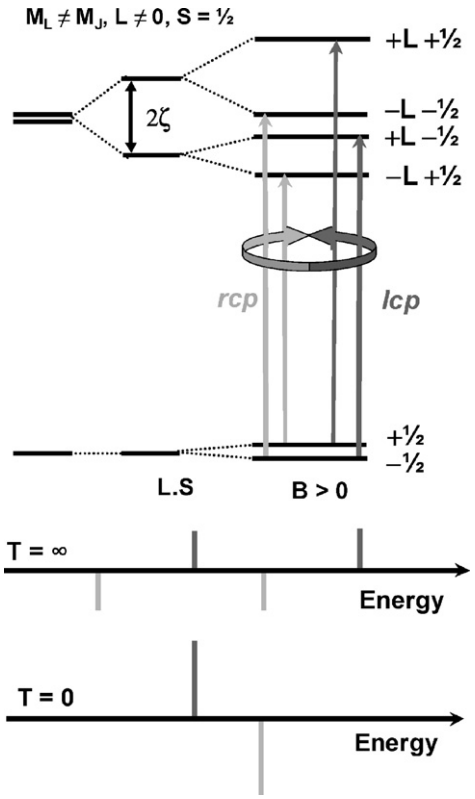

Fig. 31. The origin of the Faraday $\mathcal{C}_0$ term from Kramers doublets for the ground and excited states of a paramagnetic complex with $S=1/2$, a non-orbitally degenerate ground state and orbitally degenerate excited state (TOP). Temperature dependent, derivative-shaped signals can result when the ground state is orbitally nondegenerate and the excited state is orbitally degenerate (bottom).

Although it is possible in principle to derive the ground state g-factor value by measuring the $\mathcal{C}_0/\mathcal{D}_0$ ratio from method of moments analysis, this is usually not practical, since the absorption bands lack a baseline to baseline band envelope or due to overlap with bands associated with other metal centers or chromophores. It should be noted that in some instances, excited state parameters also have to be carefully considered. For example, when ground state degeneracy (and the associated Boltzmann distribution of population across microstates within an applied magnetic field) is introduced by spin degeneracy into what would otherwise be a Faraday $\mathcal{A}_1$ term, Fig. 31, a temperature dependent, derivative-shaped signal is observed for $\mathcal{C}_0$ term intensity.

The intensity mechanism for a single isotropic Kramers doublet ground state is:

$$\Delta A = 152.5 \tanh\left(\frac{g_L \mu_B B}{kT}\right)\left([m_{-1}^{AJ}]^2 - [m_{+1}^{AJ}]^2\right) \quad (28)$$

The analysis is complicated by the fact that, in the case of porphyrinoids, the molecular symmetry is usually axial rather than isotropic. The g-factor values are therefore different, parallel ($g_\parallel$), and perpendicular ($g_\perp$), to the applied field, but are averaged (g_{av}) out in solution due to random orientation.

Schatz et al. [59] demonstrated that for a D_{4h} symmetry complex with the $S=1/2$ Kramer's doublet ground states associated with low spin Fe(III) porphyrinoids, the zeroth moment of $\mathcal{C}_0$ term intensity for an axial complex with $g_x \approx g_y$ in the linear

limit is given by:

$$\langle \Delta\varepsilon \rangle_0 = \frac{K\mu_B B}{3kT} \frac{g_{||}[m_+^{AJ}]^2}{2} \tag{29}$$

where $m_+^{AJ} \equiv 1/\sqrt{2(m_x + im_y)}$. At saturation:

$$\langle \Delta\varepsilon \rangle_0 = (K[m_+^{AJ}]^2) \frac{\cosh(\alpha)}{\sinh^3(a)} \left(\frac{\sinh(2\alpha)}{4} - \frac{\alpha}{2} \right) \tag{30}$$

where K is a proportionality factor, and a is related to the degree of anisotropy in the g-factor values:

$$\frac{g_\parallel}{g} = \sigma = \cosh(\alpha) \tag{31}$$

$$\frac{1}{L} = \frac{\cosh(\alpha)}{\sinh^3(\alpha)} \left(\left(\frac{\sinh(2\alpha)}{4} - \frac{\alpha}{2} \right) - \left(\frac{\alpha}{2} \right) \right) \tag{32}$$

The ratio of the slope to the MCD intensity at saturation defined by an intercept value, I, can be used to derive the expression:

$$g_\parallel = \frac{3I}{L} \tag{33}$$

Thomson [60] subsequently demonstrated that it is possible to use magnetization curves of $\Delta\varepsilon$ plotted against $\mu_B B/2kT$, Fig. 32, based on $\mathcal{C}_0$ term temperature dependence studies at cryogenic temperatures (typically 2–50 K) and applied field strengths of 1–6 T, to derive values for $g_\parallel$ and $g_\perp$ based on the expressions:

$$g_{av} = \frac{1}{\sqrt{3}} \sqrt{g_x^2 + g_y^2 + g_z^2} \tag{34}$$

$$g_\perp = \frac{1}{\sqrt{2}} \sqrt{g_x^2 + g_y^2} \tag{35}$$

Band polarization information can also be derived since the slope of the magnetization curves should be the same for either x/y- or z-polarized transitions.

In the case of the $S = 5/2$ ground states of high spin Fe(III) complexes, there is a ZFS of the $M_S = \pm 1/2$, $\pm 2/3$, $\pm 5/2$ microstates due to spin–orbit coupling based on the axial (D) and rhombic (E) ZFS parameters within the spin Hamiltonian:

$$H = D\left(S_z^2 - \frac{1}{3}S^2 \right) + E(S_x^2 - S_y^2) \tag{36}$$

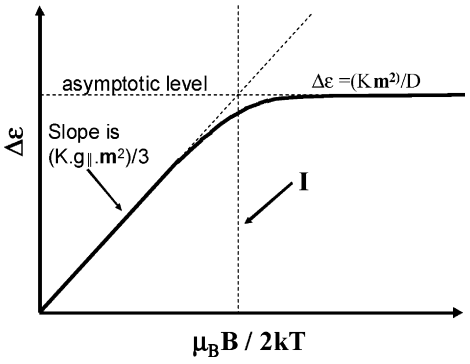

Fig. 32. Analysis of an MCD magnetization curve based on Eqs. (29)–(33).

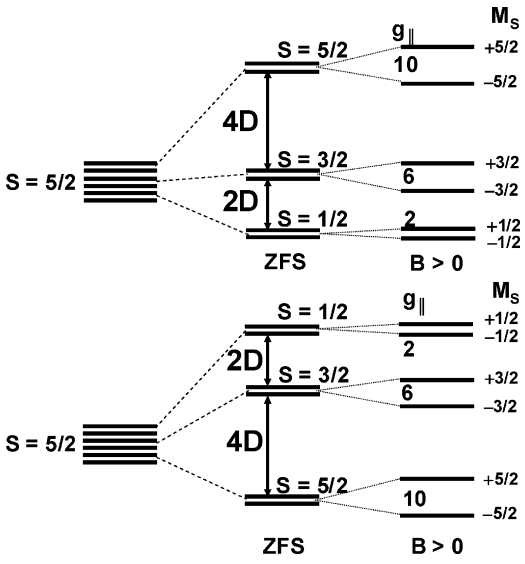

Fig. 33. The zero-field splitting of the ground state of a D_{4h} symmetry metal porphyrinoid complex with $S = 5/2$ based on the axial parameter, D. When D is positive the $S = 1/2$ microstates are stabilized (top), while if D is negative the $S = 1/2$ microstates are stabilized (bottom).

with the central metal, Fig. 33. In the early 1980s, Stephens and coworkers [7] demonstrated that the magnitude of D could be derived by fitting a plot of $\Delta\varepsilon$ against T^{-1} from cryogenic temperature MCD spectral data of a high spin Fe(III) tetraphenylporphyrin with a set of quadratic equations based on a least squares fitting approach, since the MCD signal is the sum of the MCD signals of the three sets of Kramers doublets which are populated according to a Boltzmann distribution based on the magnitude and sign of D. Study of the temperature dependence over a range where kT is comparable to the magnitude of the ZFS (typically <20 cm^{-1}) enables D to be calculated.

The Stillman group [61] subsequently used this approach to probe the ground states of horseradish peroxidase compounds I and II. The ordering of the microstates is determined by the strength of the axial ligands interaction. Compound I was found to exhibit derivative-shaped Kramers doublet based properties, Fig. 31, due to spin–orbit coupling between the low spin $S = 1$ O=Fe^{IV} central metal and an $S = 1/2$ π-cation radical porphyrinoid ligand. In contrast compound II was found to have a complex temperature dependence based on the zero field splitting of an $S = 1$ low spin O=Fe^{IV} ground state. Thomson [62] carried out studies of the pH dependence of myoglobin peroxide and found that the acidic pH form is similar to horseradish peroxidase compound II. More recently, Oganesyan and Sharonov have studied the zero field splitting parameters of the $S = 5/2$ ground states of a series of high spin Fe(III) hemes using fluoride as an axial ligand [63]. In the mid-1990s, the Faraday $\mathcal{C}_0$ term in the MCD spectra of Fe(III) phthalocyanine and its cation radical were investigated by the Stillman group [36e] based on MCD spectra recorded at different field strengths between 2.8 and 100 K. This work has been reviewed recently elsewhere and will therefore not be dealt with in detail here [34a].

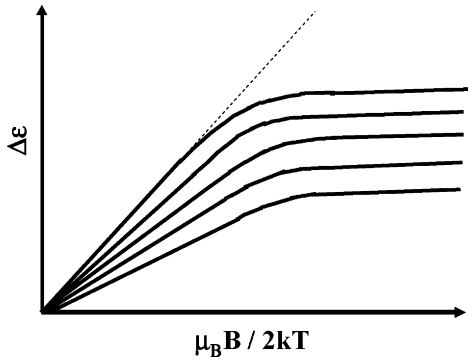

Fig. 34. When there is a non-Kramers doublet ground state, complex nested magnetization curves are observed at different temperatures and field strengths based on Eqs. (29)–(33) since $g_x \neq g_y \neq g_z$ due to the zero field splitting of the $S = 2$ ground state.

Analysis of $S = 2$ ground states associated with high spin d^6 configurations of Fe(II) are considerably more challenging than the Kramers doublet based systems which arise from d^5 configurations, since the even spin ground states are EPR silent. In 1980, Thomson and Johnson [60] reported multiple nested magnetization curves, Fig. 34, for the $S = 2$ ground state of high spin Fe(II) myoglobin but did not attempt a detailed analysis due to the complexity of the field-induced mixing of the zero-field splitting components. During the 1990s, Solomon developed techniques for analyzing variable temperature variable field (VTVF)MCD spectra for non-Kramers doublet ground states as part of a wide-ranging study of non-heme iron enzymes [64]. Solomon has demonstrated that it is possible to calculate values for the ligand field splitting properties, Δ and V, Fig. 29, of the t_{2g} set of orbitals of high spin $S = 2$ Fe(II) complexes derived from analysis of nested magnetization curves, Fig. 34, based on experimentally obtained values of the zero-field rhombic splitting of the $M_S = \pm 2$ level (δ) and $g_{\|}$.

Although the focus of this section has primarily been on iron, since it is the most important transition metal biologically, it should be noted that temperature and field dependence studies have also been carried out for porphyrinoid complexes of other transition metals such as cobalt and manganese and that the techniques described for iron can easily be applied to other metals based on the nature of the ground state [29,65].

4.5. Porphyrinoid cation and anion radicals

Additional information about the electronic structure of metal porphyrinoid complexes can be obtained through a study of their spectroelectrochemistry. Two electrons can be readily removed from the π-system HOMO, and up to four electrons added to the LUMO based on electrochemical, chemical or photochemical methods [34]. In the case of π-cation and π-anion radicals, additional $\pi \rightarrow \pi$ or $\pi^* \rightarrow \pi^*$ bands appear within the optical spectrum. When oxidation or reduction occurs at the central metal rather than in the ligand π-system, significant changes can occur in the MLCT and/or LMCT bands of transition metal complexes. EPR and MCD spectroscopy have been used extensively to study the electronic structure of porphyrinoid cation and anion radical species [36a,36j,38b].

Ideally, the validity of band assignment schemes developed on the basis of DFT calculations to account for the optical spectroscopy of a neutral porphyrinoid complex, should also be tested by studying the UV–vis absorption and MCD spectroscopy of oxidized and reduced species at room and cryogenic temperatures. The Stillman group have used spectral the results of INDO/s calculations based on DFT geometry optimizations combined with spectral band deconvolution analyses to develop a consistent band assignment scheme for the $\pi \rightarrow \pi$ or $\pi \rightarrow \pi^*$ and $\pi^* \rightarrow \pi^*$ bands of metal phthalocyanine π-cation radicals and mono-, di-, tri- and tetra-π-anionic species [36b] (Fig. 35). These studies have been reviewed elsewhere [33b–d] and will therefore not be dealt with in detail here.

Aggregation effects can complicate the study of anion and cation radical species since dimerization resulting in diamagnetic species with no EPR signal [36g,36h,66]. Based on group theory considerations, the addition of an electron to the LUMO of a porphyrinoid π-system would result in an orbitally degenerate ^2E_g ground state and attempts were made to interpret UV–vis absorption data on this basis [67]. No $1/kT$ temperature

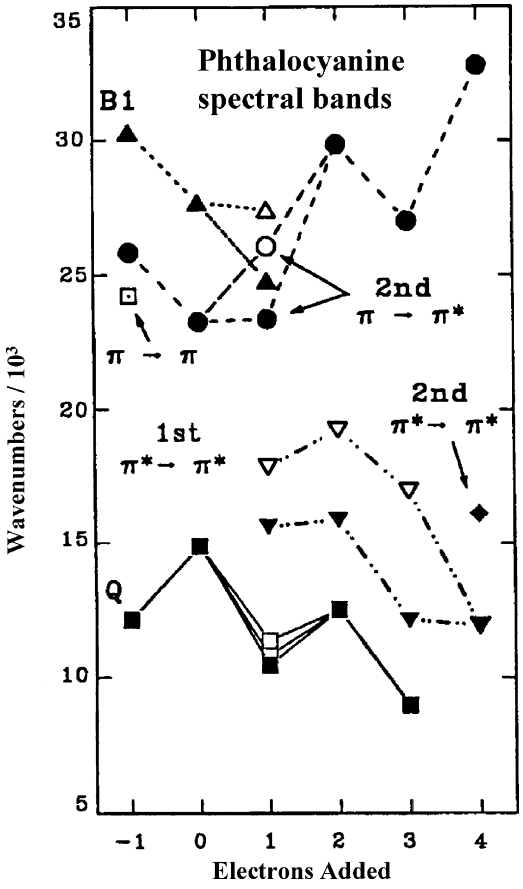

Fig. 35. The energy of the major $\pi \rightarrow \pi$ or $\pi \rightarrow \pi^*$ and/or $\pi^* \rightarrow \pi^*$ bands of neutral zinc phthalocyanine and cation and anion species based on a band assignment scheme developed on the basis of MCD spectral data and INDO/s calculations. Reproduced with permission from Ref. [36b], copyright 1997 American Chemical Society.

dependence was observed when room and low temperature MCD spectra were subsequently recorded for $[ZnPc(-3)]^-$ [36a,38b]. This provided definitive and unambiguous spectroscopic evidence that the orbitally degenerate ground states of porphyrinoid anion radicals are subject to a static Jahn–Teller distortion effect at zero-field, which lifts the orbital degeneracy, since Faraday $\mathcal{C}_0$ terms would be observed if orbital degeneracy was retained.

The spectrum is, instead, dominated by coupled oppositely signed Faraday $\mathcal{B}_0$ terms. We recently reported that the analysis of the optical spectra of the anion radical species of zinc 1, 4, 8, 11, 15, 18, 22, 25-octafluoro-2, 3, 9, 10, 16, 17, 23, 24-octaperfluoro-isopropylphthalocyanine is only possible after careful analysis of the coupled oppositely-signed Faraday $\mathcal{B}_0$ terms within the MCD spectrum [38b].

5. Conclusions

The aim of this review is to enable the broader audience of chemists to develop a deeper appreciation of MCD spectroscopy by providing the basic background material. The conceptual problems faced due to the differing definitions for left- and right-handedness that were adopted by physicists for magnetism and within classical optics are clearly a matter that can ultimately only be addressed by bodies such as IUPAC. Within the field of MCD spectroscopy, however, we strongly that the conventions recommend by Stephens et al. [7] for the three Faraday terms and the general MCD intensity equations are adopted by all research groups active within the field and that the use of the older conventions that were developed primarily for the obsolete MORD technique be discontinued.

In the end, the value of any technique rests on the value of the information provided. Once the theory on which the MCD technique is based is understood, reference to the many papers describing analysis of MCD spectral data clearly demonstrates that the MCD technique is and will continue to be a valuable spectroscopic probe for molecules and metal complexes of high symmetry. However, even when the symmetry is lowered substantially, such as in the case of chlorophyll, the OAM properties associated with the ring current of the heteroaromatic π-system determine the optical transitions within the readily accessible UV–vis–near IR regions and can be analyzed based on Michl's perimeter model approach. In the case of metal containing proteins, MCD spectroscopy has the key advantage, over other techniques used to study bulk magnetic properties of an entire sample, that spectral bands associated with specific metal centers can be studied in isolation.

Acknowledgements

This research was partially supported by the Japanese Ministry of Education, Science, Sports and Culture, a Grant-in-Aid for the COE project, Giant Molecules and Complex Systems, 2006 (to NK) and by NSERC of Canada for Operating and Equipment grants (to MJS). We thank Fujitsu America Inc. for providing the CAChe Workstation software (to MJS). MJS is a member of the Centre for Chemical Physics at UWO.

References

[1] (a) http://www.uwo.ca/chem/people/faculty/stillman.htm;
(b) http://www.chem.tohoku.ac.jp/labo/kinoubunsi/e.html.
[2] (a) D. Dolphin (Ed.), The Porphyrins, Academic Press, New York, 1978;
(b) D. Dolphin, Ann. NY Acad. Sci. 206 (1973);
(c) K.M. Kadish, K.M. Smith, R. Guilard (Eds.), The Porphyrin Handbook, Academic Press, New York, 1999;
(d) C.C. Leznoff, A.B.P. Lever (Eds.), Phthalocyanine. Principles and Properties, vols. 1–4, VCH Publications, New York, 1996.
[3] (a) R. Paolesse, in: K.M. Kadish, K.M. Smith, R. Guilard (Eds.), The Porphyrin Handbook, vol. 2, Academic Press, London, 2000, p. 201 (chapter 11);
(b) C. Erben, S. Will, K.M. Kadish, in: K.M. Kadish, K.M. Smith, R. Guilard (Eds.), The Porphyrin Handbook, vol. 2, Academic Press, London, 2000, p. 232 (chapter 11).
[4] N. Kobayashi, in: K.M. Kadish, K.M. Smith, R. Guilard (Eds.), The Porphyrin Handbook, vol. 2, Academic Press, London, 2000, p. 301.
[5] (a) C. Houssier, K. Sauer, J. Am. Chem. Soc. 92 (1970) 779;
(b) J. Deisenhofer, J.R. Norris (Eds.), The Photosynthetic Reaction Center, Academic Press, San Diego, 1993;
(c) S. Fukuzumi, Pure Appl. Chem. 75 (2003) 577.
[6] (a) J.H. Dawson, D.M. Dooley, in: A.B.P. Lever, H.B. Gray (Eds.), Iron Porphyrins, vol. 4, VCH, London, 1989, p. 1;
(b) J. Cheek, J. Dawson, in: K.M. Kadish, K.M. Smith, R. Guilard (Eds.), The Porphyrin Handbook, vol. 7, Academic Press, New York, 2000, p. 339;
(c) M.L. Kirk, K. Peariso, Curr. Opin. Chem. Biol. 7 (2003) 20;
(d) E.I. Solomon, E.G. Pavel, K.E. Loeb, C. Campochiaro, Coord. Chem. Rev. 144 (1995) 369.
[7] (a) P.J. Stephens, Adv. Chem. Phys. 35 (1976) 197;
(b) S.B. Piepho, P.N. Schatz, Group Theory in Spectroscopy with Applications to Magnetic Circular Dichroism, Wiley, New York, 1983.
[8] W.T. Simpson, J. Chem. Phys. 17 (1949) 1218.
[9] (a) J.R. Platt, J. Chem. Phys. 17 (1949) 484;
(b) J.R. Platt, in: A. Hollander (Ed.), Radiation Biology, vol. III, McGraw-Hill Book Co., New York, 1956 (chapter 2).
[10] (a) W. Moffitt, J. Chem. Phys. 22 (1954) 320;
(b) W. Moffitt, J. Chem. Phys. 22 (1954) 1820.
[11] (a) M. Gouterman, J. Chem. Phys. 30 (1959) 1139;
(b) M. Gouterman, J. Mol. Spectrosc. 6 (1961) 138;
(c) A.J. McHugh, M. Gouterman, C. Weiss Jr., Theor. Chim. Acta 24 (1972) 346;
(d) M. Gouterman, in: D. Dolphin (Ed.), The Porphyrins, vol. III, Academic Press, New York, 1978, p. 1, part A;
(e) A.M. Schaffer, M. Gouterman, E.R. Davidson, Theor. Chim. Acta 30 (1973) 9.
[12] (a) J. Michl, J. Am. Chem. Soc. 100 (1978) 6801 (and the other 16 articles within the same issue);
(b) J. Michl, Pure Appl. Chem. 52 (1980) 1549.
[13] T.D. Lash, in: K.M. Kadish, K.M. Smith, R. Guilard (Eds.), The Porphyrin Handbook, vol. 2, Academic Press, London, 2000, p. 125 (chapter 10).
[14] P. Atkins, J. de Paula (Eds.), Atkins' Physical Chemistry, Oxford University Press, Oxford, 2004.
[15] E. Charney (Ed.), The Molecular Basis of Optical Activity. Optical Rotatory Dispersion and Circular Dirchroism, John Wiley & Sons, New York, 1979.
[16] (a) P. Zeeman, Phil. Mag. 43 (1897) 226;
(b) P. Zeeman, Nobel Lectures, Physics 1901–1921, Elsevier Publishing Company, Amsterdam, 1967.
[17] (a) M. Faraday, Phil. Mag. 28 (1846) 294;
(b) M. Faraday, Phil. Trans. R. Soc. Lond. (1846) 1.
[18] G.W. Canters, J.H. van der Waals, in: D. Dolphin (Ed.), The Porphyrins, vol. III, Academic Press, New York, 1978, p. 531, part A.
[19] (a) V.E. Shashoua, J. Am. Chem. Soc. 87 (1965) 4044;
(b) M.V. Volkenstein, J.A. Sharanov, A.K. Shemelin, Nature 209 (1966) 709;
(c) V.E. Shashoua, J. Am. Chem. Soc. 86 (1964) 2109;
(d) B. Briat, Compt. Rend. 259 (1964) 2408.

[20] (a) P.J. Stephens, Inorg. Chem. 4 (1965) 1690;
(b) P.J. Stephens, J. Phys. Chem. 43 (1965) 4444.
[21] P.J. Stephens, W. Süetaka, P.N. Schatz, J. Chem. Phys. 44 (1966) 4592.
[22] A.D. Buckingham, P.J. Stephens, Ann. Rev. Phys. Chem. 17 (1966) 399.
[23] R. Serber, Phys. Rev. 41 (1932) 489.
[24] C.H. Henry, S.E. Schatterly, C.P. Slichter, Phys. Rev. A 137 (1965) 583.
[25] (a) P.N. Schatz, A.J. McCaffery, W. Süetaka, G.N. Henning, A.B. Ritchie, P.J. Stephens, J. Chem. Phys. 45 (1966) 722;
(b) B. Briat, D.A. Schooley, R. Records, E. Bunnenberg, C. Djerassi, J. Am. Chem. Soc. 89 (1967) 6170;
(c) P.N. Schatz, A.J. McCaffery, Q. Rev. Chem. Soc. 23 (1969) 552.
[26] D.D. Shillady, C.M. Castevens, C. Trindle, J. Sulik, P. Klonowski, Biophys. Chem. 105 (2003) 471.
[27] (a) J. Dobkowski, V. Galievsky, A. Starukhin, E. Vogel, J. Waluk, J. Phys. Chem. A 102 (1998) 4996;
(b) A. Gorski, B. Lament, J.M. Davis, J.L. Sessler, J. Waluk, J. Phys. Chem. A 105 (2001) 4992;
(c) A. Gorski, E. Vogel, J.L. Sessler, J. Waluk, J. Phys. Chem. A 106 (2002) 8139.
[28] (a) P.J. Stephens, J. Chem. Phys. 52 (1970) 3489;
(b) P.J. Stephens, Ann. Rev. Phys. Chem. 25 (1974) 201.
[29] B.E. Williamson, T.C. VanCott, M.E. Boyle, G.C. Misener, M.J. Stillman, P.N. Schatz, J. Am. Chem. Soc. 114 (1992) 2412.
[30] J.D. Watson, F.H.C. Crick, Nature 171 (1953) 737.
[31] A.H. Corwin, A.B. Chivvis, R.W. Poor, D.G. Whitten, E.W. Baker, J. Am. Chem. Soc. 90 (1968) 6577.
[32] A. Ceulemans, W. Oldenhof, C. Görller-Walrand, L.G. Vanquickenborne, J. Am. Chem. Soc. 108 (1986) 1155.
[33] G. Barth, R.E. Linder, E. Bunnenberg, C. Djerassi, L. Seamans, A. Moscowitz, J. Chem. Soc. Perkin II (1974) 1706.
[34] (a) M.J. Stillman, T. Nyokong, in: C.C. Leznoff, A.B.P. Lever (Eds.), Phthalocyanine. Principles and Properties, vol. 1, VCH Publications, New York, 1989, p. 133;
(b) M.J. Stillman, in: C.C. Leznoff, A.B.P. Lever (Eds.), Phthalocyanine. Principles and Properties, vol. 3, VCH Publications, New York, 1993, p. 227;
(c) J. Mack, M.J. Stillman, in: K.M. Kadish, K.M. Smith, R. Guilard (Eds.), Handbook of Porphyrins and Related Macrocycles, vol. 16, Academic Press, New York, 2003, p. 43;
(d) J. Mack, M.J. Stillman, Coord. Chem. Rev. 219–221 (2001) 993.
[35] M.J. Stillman, A.J. Thomson, J. Chem. Soc. Faraday Trans. II 70 (1974) 805.
[36] (a) J. Mack, M.J. Stillman, J. Am. Chem. Soc. 116 (1994) 1292;
(b) J. Mack, M.J. Stillman, Inorg. Chem. 36 (1997) 413;
(c) T. Nyokong, Z. Gasyna, M.J. Stillman, Inorg. Chem. 26 (1987) 1087;
(d) E.A. Ough, M.J. Stillman, Inorg. Chem. 33 (1994) 573;
(e) E.A. Ough, M.J. Stillman, Inorg. Chem. 34 (1995) 4317;
(f) T. Nyokong, Z. Gasyna, M.J. Stillman, Inorg. Chem. 26 (1987) 548;
(g) E.A. Ough, T. Nyokong, K.A.M. Creber, M.J. Stillman, Inorg. Chem. 27 (1988) 2724;
(h) E.A. Ough, Z. Gasyna, M.J. Stillman, Inorg. Chem. 30 (1991) 2301;
(i) J. Mack, M.J. Stillman, J. Phys. Chem. 95 (1995) 7935;
(j) Z. Gasyna, W.R. Browett, M.J. Stillman, Inorg. Chem. 27 (1988) 4619;
(k) T. Nyokong, Z. Gasyna, M.J. Stillman, Inorg. Chim. Acta 112 (1986) 11.
[37] (a) W.R. Browett, M.J. Stillman, Inorg. Chim. Acta 49 (1981) 69;
(b) Z. Gasyna, W.R. Browett, T. Nyokong, R. Kitchenham, M.J. Stillman, Chem. Intell. Lab. Syst. 5 (1989) 233;
(c) J. Mack, PhD Thesis, University of Western Ontario, 1994.
[38] (a) N. Kobayashi, J. Mack, K. Ishii, M.J. Stillman, Inorg. Chem. 41 (2002) 5350;
(b) S.P. Keizer, J. Mack, B.A. Bench, S.M. Gorun, M.J. Stillman, J. Am. Chem. Soc. 125 (2003) 7067;
(c) N. Kobayashi, F. Furuya, G.-C. Yug, H. Wakita, M. Yokomizo, N. Ishikawa, Chem. Eur. J. 8 (2002) 1474;
(d) N. Kobayashi, T. Fukuda, J. Am. Chem. Soc. 124 (2002) 8021;
(e) N. Kobayashi, T. Fukuda, D. Lelievre, Inorg. Chem. 39 (2000) 3632;
(f) E.A. Makarova, T. Fukuda, E.A. Luk'yanets, N. Kobayashi, Chem. Eur. J. 11 (2005) 1235;
(g) H. Ogata, T. Fukuda, K. Nakai, Y. Fujimura, S. Neya, P.A. Stuzhin, N. Kobayashi, Eur. J. Inorg. Chem. 8 (2004) 1621;
(h) H. Miwa, K. Ishii, N. Kobayashi, Chem. Eur. J. 10 (2004) 4422;
(i) N. Kobayshi, H. Miwa, V.N. Nemykin, J. Am. Chem. Soc. 124 (2002) 8007.
[39] J. Mack, Y. Asano, N. Kobayashi, M.J. Stillman, J. Am. Chem. Soc. 127 (2005) 17697.
[40] (a) J.D. Keegan, A.M. Stolzenberg, Y.C. Lu, R.E. Linder, G. Barth, A. Moscowitz, E. Bunnenberg, C. Djerassi, J. Am. Chem. Soc. 104 (1982) 4305;
(b) J.D. Keegan, A.M. Stolzenberg, Y.C. Lu, R.E. Linder, G. Barth, A. Moscowitz, E. Bunnenberg, C. Djerassi, J. Am. Chem. Soc. 104 (1982) 4317;
(c) C. Djerassi, Y. Lu, A. Waleh, A.Y.L. Shu, R.A. Goldbeck, L.A. Kehres, C.W. Crandell, A.G.H. Wee, A. Knierzinger, R. Gaete-Holmes, G.H. Loew, P.S. Clezy, E. Bunnenberg, J. Am. Chem. Soc. 106 (1984) 4241;
(d) R.A. Goldbeck, Acc. Chem. Res. 21 (1988) 95.
[41] K. Ishii, N. Kobayashi, T. Matsuo, M. Tanaka, A. Sekiguchi, J. Am. Chem. Soc. 123 (2001) 5356.
[42] M.H. Perrin, J. Phys. Chem. 59 (1973) 2090.
[43] R.G. Parr, W. Wang (Eds.), Density-Functional Theory of Atoms and Molecules, Oxford University Press, Oxford, 1989.
[44] (a) E.K.U. Gross, J.F. Dobson, M. Petersilka, in: R.F. Nalewajski (Ed.), Topics in Current Chemistry, vol. 181, Springer, Berlin, 1996, p. 81;
(b) R. Van Leeuwen, Int. J. Mod. Phys. B 15 (2001) 1969.
[45] L. Guo, D.E. Ellis, B.M. Hoffman, Y. Ishikawa, Inorg. Chem. 35 (1996) 5304.
[46] A. Ghosh, Curr. Opin. Chem. Biol. 7 (2003) 110.
[47] Gaussian, Inc., Gaussian, Inc. 340 Quinnipiac Street, Building 40, Wallingford, CT 06492.
[48] (a) P.J. Stephens, F.J. Devlin, J.R. Cheeseman, M.J. Frisch, J. Phys. Chem. A 105 (2001) 5356;
(b) B. Mennucci, J. Tomasi, R. Cammi, J.R. Cheeseman, M.J. Frisch, F.J. Devlin, S. Gabriel, P.J. Stephens, J. Phys. Chem. A 106 (2002) 6102;
(c) S. Grimme, Chem. Phys. Lett. 339 (2001) 380;
(d) S. Grimme, F. Furche, R. Ahlrichs, Chem. Phys. Lett. 361 (2002) 321;
(e) J. Autschbach, S. Patchkovskii, T. Ziegler, S.J.A. van Gisbergen, E.J. Baerends, J. Chem. Phys. 117 (2002) 581;
(f) K. Ruud, T. Helgaker, Chem. Phys. Lett. 352 (2002) 533;
(g) F. Furche, R. Ahlrichs, C. Wachsmann, E. Weber, A. Sobanski, F. Vogtle, S. Grimme, J. Am. Chem. Soc. 122 (2002) 1717;
(h) J. Autschbach, T. Ziegler, S.J.A. van Gisbergen, E.J. Baerends, J. Chem. Phys. 116 (2002) 6930.
[49] (a) J. Autschbach, T. Ziegler, J. Chem. Phys. 116 (2002) 891;
(b) M. Seth, T. Ziegler, A. Banerjee, J. Autschbach, S.J.A. van Gisbergen, E.J. Baerends, J. Chem. Phys. 120 (2004) 10942.
[50] E.J. Baerends, G. Ricciardi, A. Rosa, S.J.A. van Gisbergen, Coord. Chem. Rev. 230 (2002) 5.
[51] P.-O. Löwdin, J. Chem. Phys. 18 (1950) 365.
[52] J. Lindenberg, Chem. Phys. Lett. 1 (1967) 39.
[53] E.H. Kintner, J.H. Dawson, Inorg. Chem. 30 (1991) 4892.
[54] (a) J. Mack, C. Vermeiren, D.E. Heinrichs, M.J. Stillman, Biochem. Biophys. Res. Commun. 320 (2004) 781;
(b) C. Vermeiren, M. Pluym, J. Mack, D.E. Heinrichs, M.J. Stillman, Biochemistry (2006), in press.
[55] S. Eakanunkul, G.S.L.-R. Sumithran, A. Ghosh, K.R. Rodgers, J.H. Dawson, A. Wilks, Biochemistry 44 (1995) 13179.
[56] (a) A.J. Thomson, P.M.A. Gadsby, J. Chem. Soc. Dalton Trans. (1990) 1921;
(b) P.M.A. Gadsby, A.J. Thomson, J. Am. Chem. Soc. 112 (1990) 5003.
[57] (a) J.C. Cheng, G.A. Osborne, P.J. Stephens, W.A. Eaton, Nature (London) 241 (1973) 193;
(b) R. Rawlings, P.J. Stephens, L.A. Nafie, M.D. Kamen, Biochemistry 16 (1977) 1729.
[58] (a) N. Kobayashi, T. Nozawa, M. Hatano, Bull. Chem. Soc. Jpn. 54 (1981) 919;

(b) T. Yamamoto, T. Nozawa, N. Kobayashi, M. Hatano, Bull. Chem. Soc. Jpn. 55 (1982) 3059.
[59] P.N. Schatz, R.L. Mowery, E.R. Krausz, Mol. Phys. 35 (1978) 1537.
[60] A.J. Thomson, M.K. Johnson, Biochem. J. 191 (1980) 411.
[61] W.R. Browett, Z. Gasyna, M.J. Stillman, J. Am. Chem. Soc. 110 (1987) 3633.
[62] N. Foot, P.M.B. Gadsby, C. Greenwood, A.J. Thomson, Biochem. J. 261 (1989) 515.
[63] (a) V.S. Oganesyan, Y.A. Sharonov, Spectrochim. Acta A 53 (1997) 433;
(b) V.S. Oganesyan, Y.A. Sharonov, Biochim. Biophys. Acta 1429 (1998) 163.
[64] (a) E.I. Solomon, Chem. Rev. 100 (2000) 235;
(b) M.L. Neidig, M. Kavana, G.R. Moran, E.I. Solomon, J. Am. Chem. Soc. 126 (2004) 4486.
[65] Z. Gasyna, W.R. Browett, M.J. Stillman, Inorg. Chem. 27 (1988) 4619.
[66] J. Mack, N. Kobayashi, C.C. Leznoff, M.J. Stillman, Inorg. Chem. 36 (1997) 5624.
[67] P.C. Minor, M. Gouterman, A.B.P. Lever, Inorg. Chem. 24 (1985) 1894.
[68] Fujitsu America Inc., CAChe Scientific, 15244 NW Greenbrier Pkwy, Beaverton, OR 97006-5764.